GL021360

Episodic caldera volcanism in the Miocene southwestern Nevada volcanic field: Revised stratigraphic framework, $^{40}Ar/^{39}Ar$ geochronology, and implications for magmatism and extension

DAVID A. SAWYER *U.S. Geological Survey, M.S. 913, Denver, Colorado 80225*
R. J. FLECK, M. A. LANPHERE *U.S. Geological Survey, M.S. 937, 345 Middlefield Road, Menlo Park, California 94025*
R. G. WARREN, D. E. BROXTON *EES-1, M.S. D462, Los Alamos National Laboratory, Los Alamos, New Mexico 87545*
MARK R. HUDSON *U.S. Geological Survey, M.S. 913, Denver, Colorado 80225*

ABSTRACT

The middle Miocene southwestern Nevada volcanic field (SWNVF) is a classic example of a silicic multicaldera volcanic field in the Great Basin. More than six major calderas formed between >15 and 7.5 Ma. The central SWNVF caldera cluster consists of the overlapping Silent Canyon caldera complex, the Claim Canyon caldera, and the Timber Mountain caldera complex, active from 14 to 11.5 Ma and centered on topographic Timber Mountain. Locations of calderas older than the Claim Canyon caldera source of the Tiva Canyon Tuff are uncertain except where verified by drilling. Younger peralkaline calderas (Black Mountain and Stonewall Mountain) formed northwest of the central SWNVF caldera cluster. We summarize major revisions of the SWNVF stratigraphy that provide for correlation of lava flows and small-volume tuffs with the widespread outflow sheets of the SWNVF.

New laser fusion $^{40}Ar/^{39}Ar$ isotopic ages are used to refine and revise the timing of eruptive activity in the SWNVF. The use of high-sensitivity mass spectrometry allowed analysis of submilligram-sized samples with analytical uncertainties of ~0.3% (1σ), permitting resolution of age differences as small as 0.07 Ma. These results confirm the revised stratigraphic succession and document a pattern of episodic volcanism in the SWNVF. Major caldera episodes (Belted Range, Crater Flat, Paintbrush, Timber Mountain, and Thirsty Canyon Groups) erupted widespread ash-flow sheets within 100–300 k.y. time spans, and pre- and post-caldera lavas erupted within 100–300 k.y. of the associated ash flows. Peak volcanism in the SWNVF occurred during eruption of the Paintbrush and Timber Mountain Groups, when over 4500 km^3 of metaluminous magma was erupted in two episodes within 1.35 m.y., separated by a 750 k.y. magmatic gap. Peralkaline and metaluminous magmatism in the SWNVF overlapped in time and space. The peralkaline Tub Spring and Grouse Canyon Tuffs erupted early, and the peralkaline Thirsty Canyon Group tuffs and Stonewall Flat Tuff erupted late in the history of the SWNVF, flanking the central, volumetrically dominant peak of metaluminous volcanism. Magma chemistry transitional between peralkaline and metaluminous magmas is indicated by petrographic and chemical data, particularly in the overlapping Grouse Canyon and Area 20 calderas of the Silent Canyon caldera complex.

Volcanism in the SWNVF coincided with the Miocene peak of extensional deformation in adjoining parts of the Great Basin. Although regional extension was concurrent with volcanism, it was at a minimum in the central area of the SWNVF, where synvolcanic faulting was dominated by intracaldera deformation. Significant stratal tilting and paleomagnetically determined dextral shear affected the southwestern margin of the SWNVF between the Paintbrush and Timber Mountain caldera episodes. Larger magnitude detachment faulting in the Bullfrog Hills, southwest of the central SWNVF caldera cluster, followed the climactic Timber Mountain caldera episode. Postvolcanic normal faulting was substantial to the north, east, and south of the central SWNVF caldera cluster, but the central area of peak volcanic activity remained relatively unextended in postvolcanic time. Volcanism and extension in th SWNVF area were broadly concurrent, b in detail they were episodic in time and n coincident in space.

INTRODUCTION

The southwestern Nevada volcanic fiel (SWNVF) is an outstanding example of multicaldera silicic volcanic field. Th SWNVF has been the focus of intensive sc entific study over the past 35 yr, largely as result of underground nuclear testing at th Nevada Test Site (NTS) and nuclear-wast repository studies at Yucca Mountain. It well exposed due to Basin and Range faul ing and dissection in an arid environmen and it is well known geometrically due t hundreds of deep drill holes (>600 depth). The history of geologic investig tions of the volcanic field was recently sun marized by Byers and others (1989). Ge chronology of the volcanic rocks of the fiel was first determined by K-Ar methods (Kis ler, 1968). We report initial results of a ne generation of isotopic ages determined b the laser-fusion $^{40}Ar/^{39}Ar$ method (Da rymple and Duffield, 1988) for the princip SWNVF stratigraphic units, and we us these results to confirm significant revisio in the stratigraphic framework of th SWNVF and precisely define episodes major eruptive activity. Source calderas fc the major ash-flow sheets are described fc calderas that are well known on the basis outcrop or drill-hole data. Finally, we sun marize the implications of the high-prec sion ages for the magmatic evolution of th SWNVF, and the temporal and spatial di tribution of extensional deformation rel tive to SWNVF magmatism.

Geological Society of America Bulletin, v. 106, p. 1304–1318, 6 figs., 3 tables, October 1994.

TABLE 1. SUMMARY OF MAJOR STRATIGRAPHIC UNITS OF THE SOUTHWESTERN NEVADA VOLCANIC FIELD

Assemblage symbol	*Current name*	*Age (Ma)*	*Estimated erupted magma volumes (km^3)*	*Old (previous usage)*	*Volcanic center*
Ts	Stonewall Flat Tuff		125		Stonewall Mountain volcanic center
	Civet Cat Canyon Member		40		
	Spearhead Member		80		
Tt	Thirsty Canyon Group		300	Thirsty Canyon Tuff	Black Mountain caldera
	Gold Flat Tuff		20	Gold Flat Member	
	Trail Ridge Tuff		50	Trail Ridge Member	
	Pahute Mesa Tuff		100	Pahute Mesa Member	
	Rocket Wash Tuff	9.4	100	Rocket Wash Member	
Tf	Fortymile Canyon assemblage		140		Diverse vent areas
	Beatty Wash Formation*		110	Rhyolite of Beatty Wash	
Tm	Timber Mountain Group		2275	Timber Mountain Tuff	Timber Mountain Caldera Complex
	Ammonia Tanks Tuff	11.45	900	Ammonia Tanks member	Ammonia Tanks caldera
	Rainier Mesa Tuff	11.6	1200	Rainier Mesa Member	Rainier Mesa caldera
Tp	Rhyolite of the Loop	12.5	40		
	Paintbrush Group		2270	Paintbrush Tuff	
	Tiva Canyon Tuff	12.7	1000	Tiva Canyon Member	Claim Canyon caldera
	Yucca Mountain Tuff		25	Yucca Mountain Member	Claim Canyon caldera?
	Pah Canyon Tuff		35	Pah Canyon Member	Uncertain
	Topopah Spring Tuff	12.8	1200	Topopah Spring Member	Uncertain
Ta	Calico Hills Formation*	12.9	160	Tuffs and lavas of Calico Hills, Area 20	
Tw	Wahmonie Formation	13.0	90		Wahmonie volcano
Tc	Crater Flat Group		880	Crater Flat Tuff	Silent Canyon caldera complex
	Prow Pass Tuff		45	Prow Pass Member	
	Bullfrog Tuff	13.25	650	Bullfrog Member (and Stockade (Wash Tuff)	Uncertain Area 20 caldera†
	Tram Tuff		170	Tram Member	Prospector Pass caldera complex?
Tb	Belted Range Group		350	Belted Range Tuff	
	Dead Horse Flat Fm.*	13.5	120	Tuff and lava of Dead Horse Flat/volcanics of Saucer Mesa	
	Grouse Canyon Tuff	13.7			
	bedded member		210	Grouse Canyon Member	Grouse Canyon caldera†
	Comendite of Split Ridge	13.85		Tunnel bed 5	
			20	Rhyolite of Split Ridge	
Tr	Lithic Ridge Tuff	14.0	250		Uncertain
	Lava of Tram Ridge	14.0	60	Quartz latite lava and unit C tuff	
Tn	Tunnel Formation*		50	Tunnel beds 3 and 4	
Tu	*Tub Spring Tuff*	14.9	130	*Tub Spring Member*	*Uncertain*
To	Tuff of Yucca Flat	15.1	50		Uncertain
	Redrock Valley Tuff	15.25	360		Uncertain

Note: No entry in "Old" column indicates that current usage is unchanged.
*Newly defined with formal stratigraphic name.
†The Area 20 and Grouse Canyon calderas only compose the Silent Canyon caldera complex.

REVISED SWNVF STRATIGRAPHIC FRAMEWORK

Many units of the SWNVF were systematically described by Byers and others (1976a), who discussed in detail only the volcanic rocks they interpreted to be related to the Timber Mountain–Oasis Valley caldera complex. Older metaluminous stratigraphic units were described in Carr and others (1986), but no comprehensive stratigraphic discussion of the older and younger peralkaline units of the SWNVF and their relation to the metaluminous units has been published. The revised stratigraphy of the SWNVF summarized in Table 1 is based on our new petrologic and geochronologic studies.

The stratigraphic changes (Table 1), first, raise formally defined formations of previous usage (Belted Range, Crater Flat, Paintbrush, Timber Mountain, and Thirsty Canyon) to group rank. Petrographically, geochemically, and temporally related lava flows and nonwelded tuffs are associated with their regional welded ash-flow tuff sheets. Second, these well-defined, regionally correlative ash-flow sheets (members of the former formations) are raised to formation rank and given the rank term *Tuff*. Formation rank units are the Tub Spring (now separated from the Belted Range Group), Grouse Canyon, Tram, Bullfrog, Prow Pass, Topopah Spring, Pah Canyon, Yucca Mountain, Tiva Canyon, Rainier Mesa, Ammonia Tanks, Rocket Wash, Pahute Mesa, Trail Ridge, and Gold Flat Tuffs. Civet Cat Canyon and Spearhead Members of the Stonewall Flat Tuff, Wahmonie Formation, Lithic Ridge Tuff, tuff of Yucca Flat, and Redrock Valley Tuff retain the same rank as assigned in the earlier literature (Byers and others, 1976a; Noble and others, 1984; Carr and others, 1986). Newly defined formal stratigraphic units are the Beatty Wash Formation, Calico Hills Formation, Dead Horse Flat Formation, and Tunnel Formation. The stratigraphic units of the SWNVF are described next in older to younger sequence and related to their respective volcanic centers (Table 1).

Major ash-flow sheets of the SWNVF erupted predominantly from calderas (Table 1); lava flows and minor pyroclastic deposits erupted from numerous smaller vents. General consensus exists about the location and approximate geometry of the Silent Canyon caldera complex, the Claim Canyon caldera, the Timber Mountain caldera complex, and the Black Mountain caldera (Fig. 1). Sources for units older than the Tiva Canyon Tuff are completely buried and are documented only where revealed by extensive drilling, as for the Silent Canyon caldera complex in the subsurface of Pahute Mesa (Orkild and others, 1969; Ferguson and others, 1994). Caldera sources for Topopah Spring, Tram, Lithic Ridge, Tub Spring, and Redrock Valley Tuffs remain poorly known, though various source areas have been postulated (Byers and others, 1976a;

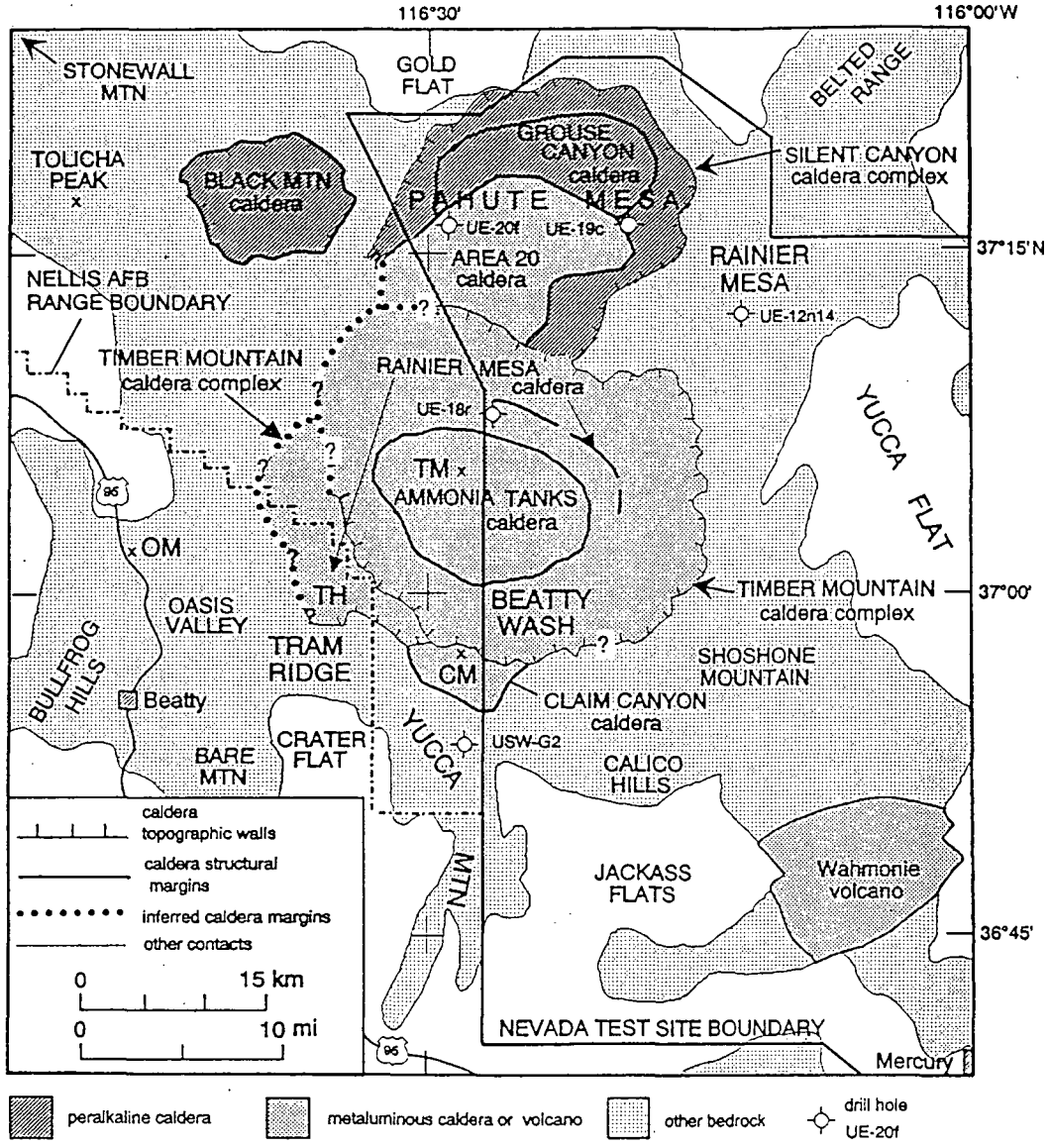

Figure 1. Location of calderas of the southwestern Nevada volcanic field (SWNVF) and index map to geographic features. Known calderas of the SWNVF are the Timber Mountain–Claim Canyon–Silent Canyon caldera complexes and the Black Mountain caldera. The Timber Mountain caldera complex was the source of the Rainier Mesa Tuff and the Ammonia Tanks Tuff. The Tiva Canyon Tuff was erupted from the Claim Canyon caldera. The Silent Canyon caldera complex consists of an earlier Grouse Canyon caldera and a younger Area 20 caldera, source of the Bullfrog Tuff. The Trail Ridge Tuff was probably erupted during the final collapse of the Black Mountain caldera, but the caldera may have largely formed in response to the eruption of the Pahute Mesa Tuff. Geographic localities mentioned in the text are abbreviated as follows: CM, Chocolate Mountain; OM, Oasis Mountain; TH, Transvaal Hills; TM, Timber Mountain.

Christiansen and others, 1977; Carr and others, 1986).

The oldest well-characterized metaluminous ash-flow sheets in the SWNVF are the Redrock Valley Tuff and the tuff of Yucca Flat (Byers and others, 1976a; Carr and others, 1986). The oldest peralkaline units in the SWNVF include the Tub Spring Tuff, previously the Tub Spring Member of the Belted Range Tuff (Sargent and others, 1964). We remove this unit from the Belted Range Group because it is 1.2 m.y. older than the Grouse Canyon Tuff and because as much as 200 m of predominantly metaluminous bedded and nonwelded tuffs of the Tunnel Formation separate the Tub Spring and the Grouse Canyon Tuffs at Rainier Mesa. Petrologic and geochemical criteria indicate that the Grouse Canyon and Tub Spring peralkaline ash-flow sheets are not comagmatic (Sawyer and Sargent, 1989). The source of the Tub Spring Tuff is unknown, and intracaldera Tub Spring has not been penetrated in Pahute Mesa, although a few drill holes penetrate the stratigraphic level of the Tub Spring.

The Tunnel Formation, as defined here, is divided into two informal subunits, beds 3 and 4, that are widely used in the Rainier Mesa area and are equivalent to tunnel beds 3 and 4 of the Oak Spring and Indian Trail Formations as used by Gibbons and others (1963) and Hansen and others (1963). The name is derived from the extensive series of tunnels used for underground nuclear testing on the east side of Rainier Mesa. The formation base overlies the top of the Tub Spring Tuff, and the top underlies the base of the bedded member of the Grouse Canyon Tuff on the east side of Rainier Mesa (bed 5 of Gibbons and others, 1963). The Tunnel Formation consists of a diverse sequence of bedded and nonwelded tuffs, predominantly rhyolitic in composition. Drill hole UE-12n14 (Fig. 1), from a depth of 351–508 m, is a reference section for the Tunnel Formation; the type section extends about 1500 m east-northeast from UE-12n14, across the east face of Rainier Mesa. Tephras in the upper part of the Tunnel Formation at Rainier Mesa probably correlate with rhyolitic to dacitic eruptive and intrusive units described below as lava of Tram Ridge. Lithic Ridge Tuff (Carr and

others, 1986) stratigraphically overlies the Tunnel Formation in the Shoshone Mountain area (Fig. 1). The lava of Tram Ridge is a sequence of lava flows and related tuff and intrusive rocks that is present beneath Lithic Ridge Tuff at Tram Ridge (Fig. 1) and as dikes around Crater Flat (quartz latite of Carr and others, 1986). The lava and tuffs correlate with the biotite-hornblende rhyolite west of Split Ridge (Byers and others, 1976b) and unit C tuff in the subsurface of Yucca Mountain (Warren and others, 1984).

The Silent Canyon caldera complex includes the oldest calderas in the SWNVF that are confidently identified. It is completely buried by younger deposits but coincides with a major gravity low (Healey, 1968; Kane and others, 1981; Healey and others, 1987). Existence of this geophysically defined caldera complex has been verified by more than 70 deep (>600 m depth) drill holes in Pahute Mesa (Ferguson and others, 1994). The composite topographic wall of the Silent Canyon caldera complex is expressed at the surface by inward dips of younger Timber Mountain tuffs that were plastered on the walls of the older caldera complex (Orkild and others, 1969; Byers and others, 1976b). The Silent Canyon caldera complex formed by two separate caldera collapses (Sawyer and Sargent, 1989): an initial collapse of the northeastern caldera of the complex related to eruption of the Grouse Canyon Tuff, and a younger collapse of the Area 20 caldera caused by eruption of the Bullfrog Tuff (Fig. 1).

The Grouse Canyon caldera was the source of the peralkaline Grouse Canyon Tuff. Comendite of Split Ridge, previously called the *rhyolite of Split Ridge* (Orkild and others, 1969; Sawyer and Sargent, 1989), is a petrologically related precursor lava to the Grouse Canyon Tuff. The bedded peralkaline tuff beneath the welded part of the Grouse Canyon Tuff is the bedded member of the Grouse Canyon Tuff, replacing *tunnel bed 5* of previous usage (Table 1). Following Grouse Canyon eruption, the northeast Silent Canyon caldera complex was filled and overflowed by postcollapse lava flows. This sequence of peralkaline lava flows and related tuffs, previously termed the *lava and tuff of Dead Horse Flat* (Orkild and others, 1969), are now assigned a formal stratigraphic rank as the Dead Horse Flat Formation, named for an open meadow in the Dead Horse Flat topographic quadrangle. The type section is drill hole UE-19c (depth 725–2249 m, Ferguson and others, in press) in Pahute Mesa (Fig. 1), where the formation overlies the Grouse Canyon Tuff and underlies the Bullfrog Tuff. The Dead Horse Flat Formation includes the extracaldera lavas exposed north of Pahute Mesa that overlie the Grouse Canyon Tuff that were termed *volcanics of Saucer Mesa* by Sawyer and Sargent (1989).

The Bullfrog Tuff is the ash-flow sheet associated with the younger Area 20 caldera (Fig. 1) of the Silent Canyon caldera complex (Sawyer and Sargent, 1989); the intracaldera facies was termed the *lithic-rich ash-flow tuff* by Orkild and others (1969) and is interleaved with thick megabreccia lenses. The intracaldera Bullfrog is more than 600 m thick in three drill holes, including UE-20f (1859–2522 m depth; Ferguson and others, 1994). Boundaries of the Area 20 caldera (Minor and others, 1993) are fixed by drill holes east and north of drill hole UE-20f, but evidence for the caldera south and west of UE-20f and UE-18r (Fig. 1) is concealed by younger units and not delineated by drilling southwest of the NTS boundary. Gravity data (Kane and others, 1981) suggest that the Area 20 caldera extends south under the Timber Mountain caldera complex. The distribution of thick Calico Hills lavas and tephras south of Timber Mountain and at Yucca Mountain is evidence of petrochemically related post–Area 20 caldera volcanism and supports the interpretation of Area 20 caldera collapse extending at least partly beneath Timber Mountain (Warren, 1983). The Stockade Wash Tuff (Byers and others, 1976a) is petrographically similar to both the outflow facies of the Bullfrog Tuff at Yucca Mountain and the intracaldera Bullfrog Tuff on Pahute Mesa. The Stockade Wash Tuff and the Bullfrog Tuff at Yucca Mountain may be separate outflow lobes of a composite ash-flow sheet that represent slightly different parts of the compositional zonation in a single magma chamber. The paleomagnetic signatures of these two geographically discrete ash-flow tuffs are identical and distinct from a typical Miocene direction (Hudson and others, 1994), consistent with eruption at the same time. For these reasons, we correlate the Stockade Wash Tuff with the Bullfrog Tuff, an important unit in the Yucca Mountain area (Warren, 1983; Broxton and others, 1989; Scott, 1990). A caldera source for the Bullfrog Tuff in Crater Flat (Carr and others, 1986) has been contested (Scott, 1990) and is inconsistent with evidence for an Area 20 caldera source.

Caldera sources for other units of the Crater Flat Group are less well known. The northern half of the proposed Prospector Pass caldera complex (near Tram Ridge, Fig. 1) is reasonably supported by field and geophysical evidence (Snyder and Carr, 1984) and may have been the source of the Tram Tuff (Carr and others, 1986). The Prow Pass Tuff does not have an identified source, and it may be small enough (Carr and others, 1986) not to have erupted from a caldera.

The Wahmonie Formation (Poole and others, 1965) is a sequence of andesite and dacite lava flows and related volcaniclastic sedimentary rocks and tephras that erupted from the Wahmonie volcano (Fig. 1) southeast of the Timber Mountain caldera complex (Frizzell and Shulters, 1990; Broxton and others, 1989). Biotite-rich mafic tephras that erupted from the Wahmonie volcano form a widespread, distinctive marker between Crater Flat Group tuffs and Calico Hills Formation tuff. This marker is common in Yucca Flat and Rainier Mesa, is exposed west of Yucca Flat and east of Yucca Mountain (Broxton and others, 1993), but is absent to the northwest in Pahute Mesa (Ferguson and others, 1994).

The Calico Hills Formation combines the tuffs and lavas of Calico Hills (significant at Yucca Mountain) with the tuffs and lavas of Area 20 (significant at Pahute Mesa). These two sequences are stratigraphically and petrologically equivalent (Warren, 1983) and resulted from Crater Flat Group postcaldera volcanism. Throughout the SWNVF they lie stratigraphically between the Wahmonie Formation (or the Crater Flat Group where Wahmonie is absent) and the Paintbrush Group. The type locality for the Calico Hills Formation is the northwestern Calico Hills (Orkild and O'Connor, 1970); reference sections are drill holes USW G-2, at 518–824 m depth at Yucca Mountain (Warren and others, 1984), and UE-20f, at 899–1324 m depth at Pahute Mesa (Ferguson and others, 1994). The Calico Hills Formation consists of rhyolite lava flows, domes, and nonwelded ash-flow and bedded tuffs. It has a maximum thickness of 1306 m and commonly is >600 m thick in western Pahute Mesa drill holes (Fig. 6, Ferguson and others, 1994); in the Yucca Mountain area it is 50–300 m thick (Warren, 1983; Warren and others, 1984; Broxton and others, 1993).

Paintbrush Group tuffs and lavas are one of the most widespread and voluminous caldera-related assemblages in the SWNVF.

Topopah Spring Tuff directly overlies bedded rhyolite tuffs of the Calico Hills Formation at Yucca Mountain and at most localities south of Timber Mountain. A caldera source for the Topopah Spring Tuff is buried and its location uncertain. The Pah Canyon Tuff may have been too small (Byers and others, 1976a) to have formed a caldera; no separate source has been identified. The younger of the widespread Paintbrush Group ash-flow sheets, the Tiva Canyon Tuff, was erupted from the Claim Canyon caldera (Byers and others, 1976a). The Claim Canyon caldera (Fig. 1) is bounded by precaldera rhyolite tuffs and lavas of the Calico Hills Formation to the southeast, and by precaldera tuffs and lavas of the Crater Flat Group to the southwest. Only part of the caldera is exposed because much of the caldera collapsed into the younger Timber Mountain caldera complex to the north (Byers and others, 1976a). The boundary illustrated is approximately the structural boundary of the resurgent intracaldera block; the topographic wall is not exposed (Christiansen and Lipman, 1965). The presence of thick intracaldera Tiva Canyon Tuff, a reversely magnetized unit, is corroborated by a negative aeromagnetic anomaly centered on Chocolate Mountain (Fig. 1); a local gravity high is consistent with the exposed Claim Canyon caldera being a fragment of the resurgent dome (Kane and others, 1981). The Yucca Mountain Tuff, directly beneath the Tiva Canyon, is an early small-volume eruption of the uppermost high-silica rhyolite part of the Tiva Canyon magma chamber (Broxton and others, 1989), probably from the same area of the Claim Canyon caldera.

Climactic ash flows of the Timber Mountain Group were erupted from the Timber Mountain caldera complex. The complex consists of two overlapping, resurgent calderas: an older caldera formed by eruption of the Rainier Mesa Tuff, and a younger, nested caldera formed by eruption of the Ammonia Tanks Tuff (Minor and others, 1993). Intracaldera Rainier Mesa Tuff and caldera-collapse breccias are exposed in the Transvaal Hills, west of Timber Mountain (Byers and others, 1976a, 1976b). These exposures and their inferred subsurface extensions coincide with aeromagnetic lows (Kane and others, 1981), consistent with the reversed remanent magnetic polarity of the Rainier Mesa Tuff (Bath, 1968). We interpret the Transvaal Hills as the western part of a larger resurgent dome formed within the Rainier Mesa caldera. The dome was later truncated and down-dropped on the east by formation of the Ammonia Tanks caldera. The Rainier Mesa caldera structural boundary is buried but can be delimited by geophysical and drill-hole data (UE-18r); the margin (Fig. 1) approximately coincides with the inferred buried cauldron boundary on the Timber Mountain caldera geologic map (Byers and others, 1976b; Minor and others, 1993).

Intracaldera Ammonia Tanks Tuff forms topographic Timber Mountain and was originally identified as the dome of the Timber Mountain caldera (Byers and others, 1976a); it is, more specifically, the resurgent dome of the Ammonia Tanks caldera (Minor and others, 1993). The structural margin or ring-fault zone of the Ammonia Tanks caldera (Fig. 1) is exposed on the east margin of Timber Mountain. The margin was depicted as a tuff dike zone on the Timber Mountain caldera geologic map (Byers and others, 1976b); its continuity as a ring-fault zone around the Ammonia Tanks resurgent dome is clearly demonstrated by subregional gravity and aeromagnetic anomalies (Kane and others, 1981).

Previous studies (Byers and others, 1976a, 1976b, 1989) depicted only the geometry of an "approximate outer cauldron boundary" and a "partial buried inner cauldron fault" for the Timber Mountain caldera complex. As has been documented for calderas in the San Juan volcanic field and many other localities (Lipman, 1984), calderas have a collapse boundary or topographic wall outside of the ring-fault or structural margin. The composite topographic wall of the Timber Mountain caldera complex (Minor and others, 1993) is exposed around 200° of the calderas (Fig. 1); it is covered by younger units on the northwest side of the complex (south and west of drill holes UE-18r and UE-20f and the NTS boundary; Byers and others, 1976b). The distinction between the Ammonia Tanks and Rainier Mesa topographic walls is uncertain along most of the length of this contact. The two collapse features can be clearly distinguished only east and south of the Transvaal Hills (Fig. 1), where the Ammonia Tanks topographic wall swings north to the east of the Transvaal Hills and the Rainier Mesa topographic wall trends west to the south of the Transvaal Hills (Minor and others, 1993) before being covered by younger gravels in Oasis Valley.

Geologic data previously cited as evidence for an Oasis Valley caldera segment (Byers and others, 1976a; Christiansen and others, 1977) are inadequate to confirm existence (Noble and others, 1991); t gravel-filled basin in Oasis Valley cannot unequivocally linked to caldera collaps from eruption of the Ammonia Tanks, Ti Canyon, or Rainier Mesa Tuffs. A lap-out Ammonia Tanks Tuff against precalde rocks at Oasis Mountain (Byers and other 1976b) is probably related to paleotopogr phy generated by syn-volcanic tectonism the Oasis Valley area (Minor and other 1993). Proposed caldera walls on the we side and north of Oasis Mountain (Bye and others, 1976b; Noble and others, 199 do not continue into the exposed Rainie Mesa and Ammonia Tanks topographi walls near Timber Mountain (Fig. 1) accord ing to existing evidence. Aeromagnetic dat (Kane and others, 1981; U.S. Geologica Survey, 1979) indicate that the arcuate neg ative magnetic anomaly associated with re versely magnetized intracaldera Rainie Mesa Tuff does not extend west to Oasi Mountain. This anomaly is the basis for th inferred (though buried) western boundar of the Rainier Mesa caldera illustrated i Figure 1. Because no unit can uniquely b attributed to it, we recommend that the con cept of an Oasis Valley caldera segment b abandoned and disassociated from the well characterized Timber Mountain calder complex formed by eruption of the Ammo nia Tanks and Rainier Mesa Tuffs. New sub surface data will be required to unambigu ously establish the origin of Oasis Valley.

The newly defined Beatty Wash Forma tion is part of an informal sequence of units the Fortymile Canyon assemblage. Assign ment of rhyolite lava flows and tuffs previ ously called the *rhyolite lavas of Fortymile Canyon* on the south side of the Timber Mountain caldera complex (Byers and others, 1976a, 1976b) has been uncertain because field relations to the major ash-flow sheets of the Timber Mountain and Paintbrush Groups are lacking. Most of these units can be correlated with the Timber Mountain and Paintbrush Groups based on detailed petrography and chemistry (Warren and others, 1988). We restrict the Fortymile Canyon assemblage to the sequence of rocks stratigraphically above the Ammonia Tanks Tuff and related lavas of the Timber Mountain Group, and beneath the peralkaline units of the Thirsty Canyon Group. This assemblage is a diverse sequence of rhyolite lava flows and domes, related tephra deposits, minor ash-flow deposits, and basaltic and other mafic lavas erupted from a variety of relatively small-volume

TABLE 2. REPRESENTATIVE $^{40}Ar/^{39}Ar$ ANALYSES

Calico Hills Formation lava/sanidine
Field sample number: RW19f2-m
Irradiation laboratory number LXXXVII:A22; J = 0.003590

Sample number	Percent $^{40}Ar^*$	^{36}Ar-Ca	$^{40}Ar/^{39}Ar$	$^{37}Ar/^{39}Ar$	$^{36}Ar/^{39}Ar$	$^{40}Ar/^{39}Ar$ Age (Ma)
90Z0582	87.6	1.29	2.2829	0.05373	0.00097	12.90 ± 0.08
90Z0583	77.4	0.54	2.5735	0.04612	0.00197	12.85 ± 0.08
90Z0584	86.6	0.47	2.3218	0.02106	0.00105	12.98 ± 0.08
90Z0585	80.2	0.53	2.4910	0.03815	0.00167	12.90 ± 0.08
90Z0586	79.1	0.62	2.5171	0.04768	0.00178	12.86 ± 0.08
90Z0587	71.8	0.23	2.7693	0.02589	0.00265	12.83 ± 0.08
			Weighted mean age and uncertainty (Ma)			
		12.89 ± 0.03		s.e.m: 0.02		MSWD: 0.458

Grouse Canyon Tuff/sanidine
Field sample number: DS18a1
Irradiation laboratory number XCIII:47; J = 0.004055

Sample number	Percent $^{40}Ar^*$	^{36}Ar-Ca	$^{40}Ar/^{39}Ar$	$^{37}Ar/^{39}Ar$	$^{36}Ar/^{39}Ar$	$^{40}Ar/^{39}Ar$ Age (Ma)
91Z0410A	90.3	1.60	2.0854	0.03953	0.00066	13.72 ± 0.09
91Z0410B	88.4	1.67	2.1246	0.05067	0.00082	13.69 ± 0.10
91Z0410C	89.4	1.69	2.1063	0.04626	0.00074	13.72 ± 0.10
91Z0410D	90.3	1.94	2.0693	0.04759	0.00066	13.62 ± 0.12
91Z0410E	79.5	0.71	2.3878	0.04309	0.00163	13.84 ± 0.14
91Z0410F	88.9	1.45	2.1031	0.04140	0.00077	13.63 ± 0.11
			Weighted mean age and uncertainty (Ma)			
		13.70 ± 0.04		s.e.m: 0.03		MSWD: 0.407

Irradiation laboratory number CII:A24; J = 0.002975

Sample number	Percent $^{40}Ar^*$	^{36}Ar-Ca	$^{40}Ar/^{39}Ar$	$^{37}Ar/^{39}Ar$	$^{36}Ar/^{39}Ar$	$^{40}Ar/^{39}Ar$ Age (Ma)
91Z1035A	98.5	9.31	2.6145	0.04548	0.00013	13.76 ± 0.08
91Z1035B	97.9	6.56	2.6190	0.04482	0.00018	13.70 ± 0.09
91Z1035C	97.9	3.07	2.6171	0.01977	0.00017	13.70 ± 0.09
91Z1035D	87.4	1.36	2.9642	0.06386	0.00126	13.85 ± 0.09
91Z1035E	97.5	6.79	2.6182	0.05635	0.00022	13.64 ± 0.10
91Z1035F	99.2	14.93	2.5990	0.03647	0.00007	13.78 ± 0.09
91Z1035G	95.3	3.24	2.6823	0.05112	0.00042	13.67 ± 0.09
91Z1035H	96.3	1.95	2.6727	0.02349	0.00032	13.76 ± 0.09
			Weighted mean age and uncertainty (Ma)			
		13.74 ± 0.03		s.e.m: 0.02		MSWD: 0.553
			Pooled weighted mean age and uncertainty (Ma)			
		13.72 ± 0.03				MSWD: 0.498

Note: MSWD is the mean square of weighted deviates; s.e.m. is the standard error of the mean; and J is the neutron flux parameter.

vent complexes. The Beatty Wash Formation is the most significant of these post–Timber Mountain units and consists of rhyolite lava domes and related pyroclastic deposits in the moat of the Ammonia Tanks caldera. The type area is upper Beatty Wash on the Topopah Spring NW quadrangle (Christiansen and Lipman, 1965); the formation also includes the related tuff of Cutoff Road to the west of the Timber Mountain caldera complex adjoining Oasis Valley (Byers and others, 1976b). The Fortymile Canyon assemblage also includes such widely dispersed units (Minor and others, 1993) as the rhyolite of Rainbow Mountain in the Beatty area (Maldonado and Hausback, 1990), the rhyolite of West Cat Canyon west of Timber Mountain, and the mafic lavas at Dome Mountain and the rhyolite lavas of Shoshone Mountain along the southeast margin of the Timber Mountain caldera complex (Byers and others, 1976b).

The Black Mountain caldera, just west of the Silent Canyon caldera complex (Fig. 1), produced the youngest widespread ash-flow sheets in the SWNVF area. Those sheets make up the several moderate-volume peralkaline ash-flow tuffs (Christiansen, 1979; Noble and others, 1984): the Rocket Wash, Pahute Mesa, Trail Ridge, and Gold Flat Tuffs (Table 1) of the Thirsty Canyon Group. Individual collapse boundaries have not been identified due to a lack of dissection of the caldera. The composite topographic wall of the Black Mountain caldera (Fig. 1) is mantled by Trail Ridge Tuff (Minor and others, 1993), indicating that collapse was syn– or pre–Trail Ridge in age. The Stonewall Mountain volcanic center (Noble and others, 1984; Minor and others, 1993) is >50 km northwest of the central SWNVF caldera cluster. Distal Stonewall tuff overlaps the Thirsty Canyon Group tuffs at Black Mountain.

$^{40}Ar/^{39}Ar$ GEOCHRONOLOGY

Ages reported here were determined at the U.S. Geological Survey laboratories in Menlo Park, California. Two $^{40}Ar/^{39}Ar$ methods (described in the Appendix) were used: laser fusion determination of small sanidine samples and incremental heating determination of larger biotite samples. Twenty-six sanidine samples were analyzed by the laser fusion $^{40}Ar/^{39}Ar$ technique (Dalrymple and Duffield, 1988; Dalrymple, 1989). Analytical results for two representative samples are listed in Table 2: RW19f2, a Calico Hills Formation sanidine from a rhyolite lava north of Timber Mountain, and DS18a1, Grouse Canyon Tuff sanidine irradiated and analyzed twice. Two biotite samples (Wahmonie Formation lava and dacite lava of Tram Ridge, Fig. 2) were analyzed by the incremental heating $^{40}Ar/^{39}Ar$ technique (Dalrymple and Lanphere, 1971; Lanphere, 1988). These biotites yielded undisturbed age plateaus containing >90% of the total gas and have atmospheric argon intercepts on $^{36}Ar/^{40}Ar$-$^{39}Ar/^{40}Ar$ isochron diagrams.

We determined $^{40}Ar/^{39}Ar$ ages for the largest volume, most widespread units of the SWNVF (Table 3). All reported ages are rounded to ±50 ka because additional results for the same units and further refinements of the monitor ages may affect the final ages by as much as 10–50 k.y. due to cumulative J-curve calibration uncertainties and within-unit and within-sample age variations. Sample locations and detailed analytical data for samples other than those listed in Table 2 and Figure 2 are available from the first author upon request. Results for four samples of Topopah Spring Tuff, three samples each of Ammonia Tanks, Rainier Mesa, and Tiva Canyon Tuffs, and two samples of Bullfrog Tuff are reported as error-weighted pooled averages for the absolute age and uncertainty. All $^{40}Ar/^{39}Ar$ ages were measured relative to a monitor age of 513.9 Ma for MMhb-1 (Lanphere and others, 1990; Dalrymple and others, 1993). The $^{40}Ar/^{39}Ar$ results presented here agree well with $^{40}Ar/^{39}Ar$ determinations recently published for a few SWNVF units (Hausback and others, 1990; Noble and others, 1991), when recalculated to the same monitor ages.

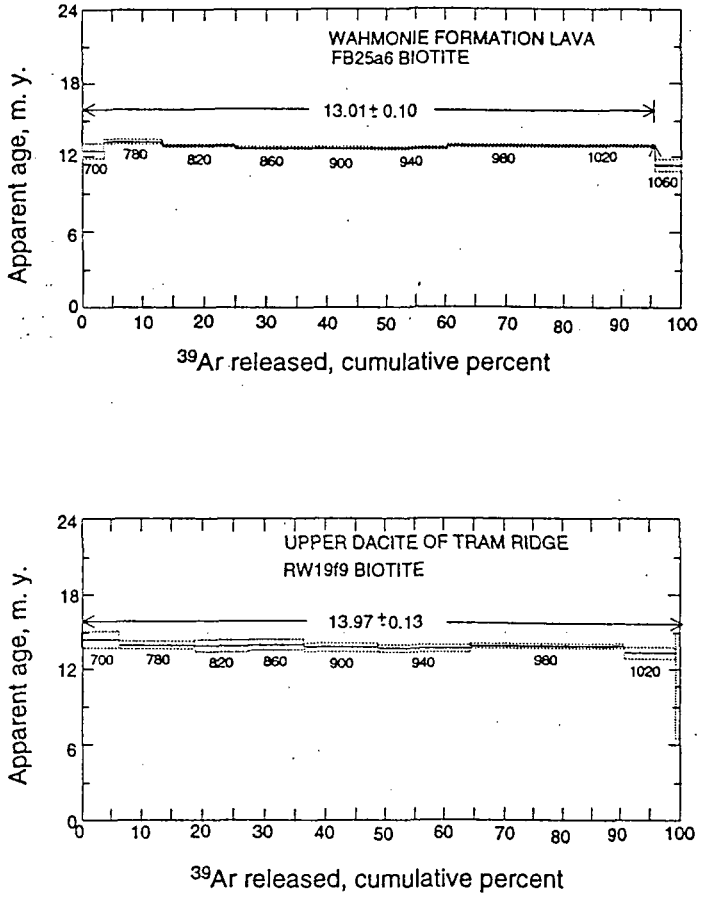

Figure 2. $^{40}Ar/^{39}Ar$ plateau age spectra for biotite from FB25a6, Wahmonie Formation lava, and from RW19f9, dacite lava of Tram Ridge.

DISCUSSION

Comparison of New $^{40}Ar/^{39}Ar$ and Previous K/Ar Results

Volcanic rocks of the SWNVF have been the subject of many conventional K/Ar geochronology studies since the early 1960s. Over 150 K/Ar determinations have been made on SWNVF units (Kistler, 1968; Marvin and others, 1970, 1973, 1989; Marvin and Cole, 1978; Weiss and others, 1989; Noble and others, 1984, 1991; R. J. Fleck, unpub. data; and F. W. McDowell, University of Texas, 1989, written commun.). Typical reported analytical uncertainties for K/Ar ages average about 3% (Kistler, 1968; Tabor and others, 1985) and thus represent absolute age uncertainties of 0.25–0.50 m.y. for the 7.5–15.25 Ma rocks of the SWNVF. Even if the ~100 units of the SWNVF, or the 20 major ash-flow sheets, or the 13 petrologic assemblages (Table 1) were distributed evenly across this time period, the ages of units would be unresolvable given a 3% uncertainty. Because the interval between eruptions was nonuniform—in fact distinctly episodic (as detailed below)—the actual overlap of uncertainties is even greater. Consequently, conventional K/Ar geochronology discriminates only three episodes of SWNVF volcanism: an early episode including all older volcanic rocks up through the Paintbrush Group (Table 1), a Timber Mountain Group episode, and a younger (but inaccurately dated by K/Ar) Thirsty Canyon Group and basalt episode.

In contrast, analytically distinct $^{40}Ar/^{39}Ar$ ages (Table 3) on SWNVF units are consistent with tight stratigraphic constraints derived from petrographic, geochemical, and field geological studies (Byers and others, 1976a; Warren and others, 1988; Broxton and others, 1989; and Sawyer and Sargent, 1989). Analytical uncertainties for laser-fusion $^{40}Ar/^{39}Ar$ on sanidine range from 20–60 k.y., about an order of magnitude better than those measured by the conventional K/Ar method. Comparison of the new ages determined by $^{40}Ar/^{39}Ar$ and those determined by K/Ar on the same mineral separate or the same unit (Fig. 3) illustrate types of problems with the K/Ar data. The K/Ar ages for sanidine are more discordant with $^{40}Ar/^{39}Ar$ ages than those for biotite. Nearly 45% of sanidine K/Ar determinations are too young by more than the typical 3% uncertainty of the method. Several explanations have been proposed for inaccurately young sanidine K/Ar ages (McDowell, 1983; Hausback and others, 1990), but young sanidine ages exhibit no simple relationship to sanidine chemical composition and are not as common as would be expected if due to a standard analytical problem. A relationship between alkali feldspar structural state and concordance of K/Ar and $^{40}Ar/^{39}Ar$ age determinations may explain the aberrant ages, as the most strongly exsolved sanidines have the most discordant ages (P. W. Lipman, U.S. Geological Survey, 1969, written commun.; F. W. McDowell, 1989, written commun.). More than half of K/Ar biotite age determinations agree

TABLE 3. $^{40}Ar/^{39}Ar$ AGE DETERMINATIONS

Unit	Sample	Mineral/N	Weighted mean age (Ma)	s.e.m.	Uncertainty
Spearhead Member	N80A	sanidine/5	7.5	0.01	0.03
Rocket Wash Tuff	Age 11	sanidine/4	9.4	0.03	0.04
Ammonia Tanks Tuff	Pooled average of 3	sanidines/19	11.45	0.03	0.03
Rainier Mesa Tuff	Pooled average of 3	sanidines/16	11.6	0.03	0.03
Rhyolite of Loop	POG2b11	sanidine/6	12.5	0.02	0.03
Tiva Canyon Tuff	Pooled average of 3	sanidines/20	12.7	0.03	0.03
Topopah Spring Tuff	Pooled average of 4	sanidines/21	12.8	0.02	0.03
Calico Hills Formation	RW19f2-m	sanidine/6	12.9	0.02	0.04
Wahmonie Formation	FB25a6	biotite-plateau/8	13.0	0.09	0.10
Bullfrog Tuff	Pooled average of 2	sanidines/13	13.25	0.02	0.04
Dead Horse Flat Formation	DS19d15	sanidine/5	13.5	0.02	0.02
Grouse Canyon Tuff	DS18a1	sanidine/14	13.7	0.02	0.04
Comendite of Split Ridge	DS19f9	sanidine/5	13.85	0.01	0.02
Lithic Ridge Tuff	TSV-417B	sanidine/5	14.0	0.07	0.06
Lava of Tram Ridge	RW19f9	biotite-plateau/7	14.0	0.35	0.13
Tub Spring Tuff	DS15e6	sanidine/5	14.9	0.01	0.04
Tuff of Yucca Flat	FB16a3	sanidine/6	15.1	0.05	0.06
Redrock Valley Tuff	Age 13	sanidine/6	15.25	0.06	0.06

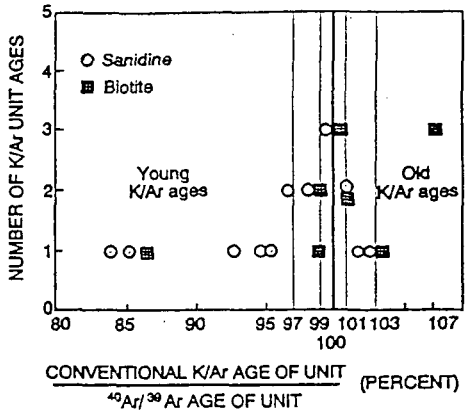

Figure 3. Comparison of laser fusion $^{40}Ar/^{39}Ar$ ages with previous conventional K-Ar ages for stratigraphic units of the southwestern Nevada volcanic field. K/Ar data are from published sources listed in text and from unpublished data provided by F. W. McDowell (1989, written commun.).

within 1% of the new $^{40}Ar/^{39}Ar$ ages, but about 30% of the K/Ar biotite ages are >3% older. A probable explanation for these older ages is that they are contaminated by xenocrysts due to fusion of large (>1 g) bulk samples.

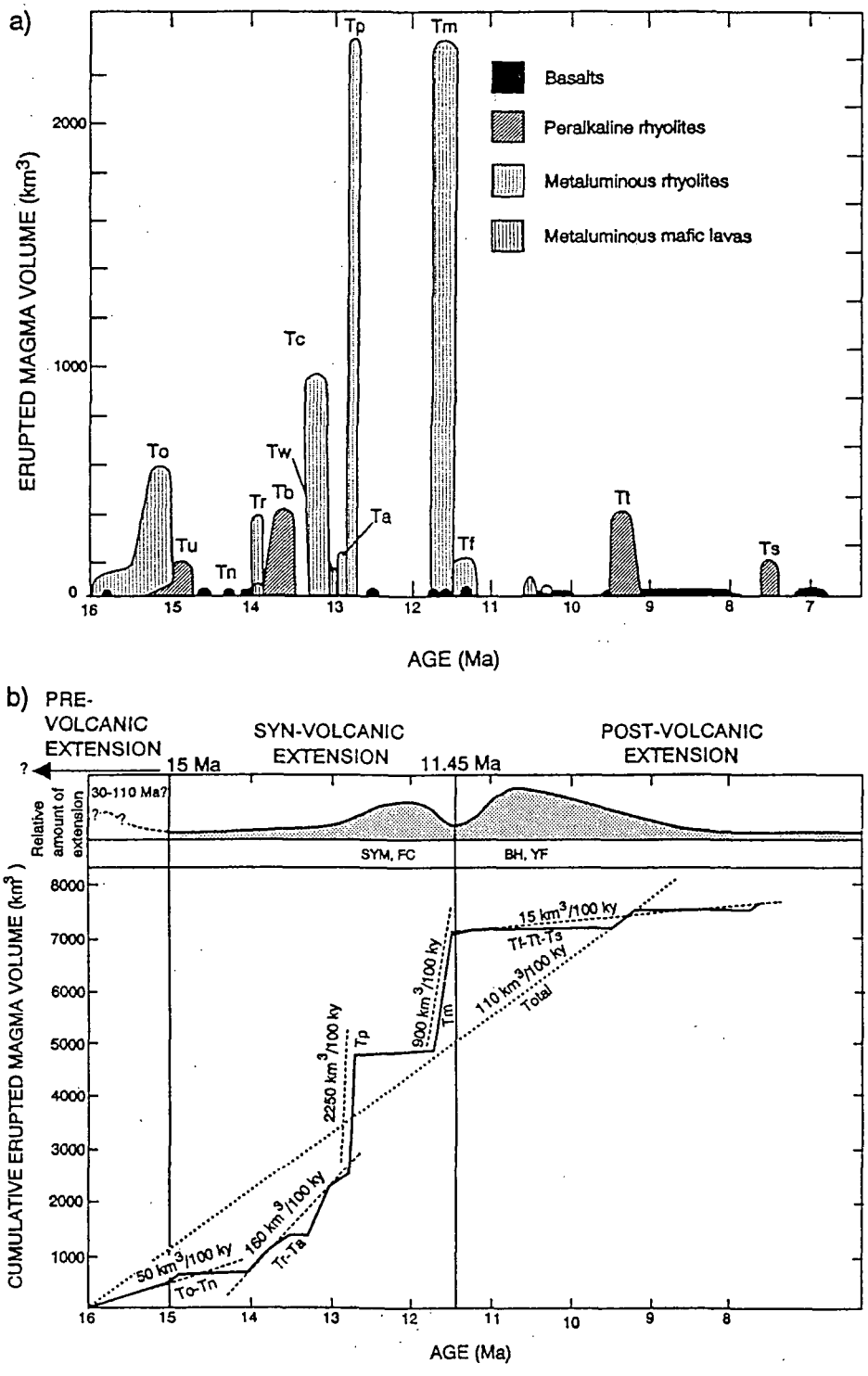

Figure 4. Episodes of volcanism in the southwestern Nevada volcanic field. (a) Approximate erupted magma volume for each group or assemblage plotted against the age range. Group or assemblage symbols and erupted magma volumes are from Table 1. Area under the curves is not proportional to volume, as width of the bars is solely a function of the age range of the assemblage. (b) Cumulative erupted magma volume and rates of material erupted for volcanic assemblages of the southwestern Nevada volcanic field (SWNVF). Top of figure superimposes episodes of extension and relative magnitude of extension during extensional episodes. Abbreviations for extensional domains described in text and illustrated in Figures 4b and 6 are SYM, southern Yucca Mountain; FC, Fluorspar Canyon; BH, Bullfrog Hills; and YF, Yucca Flat. Group or assemblage symbols as listed in Table 1. Rates of material erupted are derived graphically and listed above dashed lines. Average eruptive rate for the SWNVF over the 7 m.y. history of the field is ~110 km^3/100 k.y.

Episodicity of Caldera Volcanism

The high-resolution $^{40}Ar/^{39}Ar$ ages reveal for the first time a pattern of episodic volcanic activity in the SWNVF. This pattern is accentuated when erupted magma volumes are considered (Fig. 4a). Magma volume estimates (Table 1) are from Byers and others (1976a), Broxton and others (1989), and Sawyer and Sargent (1989) or are compiled from geologic map data (Ekren and others, 1971; Frizzell and Shulters, 1990) for units not cited in the previous sources. Volume estimates are at best semiquantitative because of the limitations of the calculation method (known area of exposure multiplied

by estimated average thickness). Volumes of major ash-flow sheets older than the Tiva Canyon Tuff have an additional significant uncertainty in that intracaldera tuff is not exposed, and thus intracaldera tuff volumes are not estimated. Volumes of the intracaldera Bullfrog and Grouse Canyon Tuffs have been estimated because they are penetrated by several drill holes in the subsurface of the Silent Canyon caldera complex. Despite these volumetric uncertainties, the general time-volume relationship is decidedly episodic (Fig. 4a).

Eruption of the Paintbrush and Timber Mountain Group magmas was the climax of volcanism in the SWNVF. Over 4500 km^3 of magma was erupted in two distinct and subequal episodes separated by a magmatic gap of 750 k.y. Each episode lasted 150 k.y. or less (Fig. 4a). Volume of the remaining units of the SWNVF was dwarfed by the magma erupted as the four large ash-flow sheets of the Paintbrush and Timber Mountain Groups. The cumulative volume of magma erupted prior to the climactic eruptions of the Paintbrush Group was about 2500 km^3 erupted over 3.3 m.y. (Fig. 4b). The volume erupted after the Timber Mountain Group was 600 km^3 over 4 m.y. during the waning of SWNVF volcanism.

The rate of material erupted gradually increased with time from the initiation of SWNVF at ca. 16 Ma to the eruption of the Paintbrush Group between 12.8 and 12.7 Ma. The first major episode of volcanism occurred between 15.25 and 14.9 Ma when the Redrock Valley Tuff (15.25 Ma), tuff of Yucca Flat (15.1 Ma), and the Tub Spring Tuff (14.9 Ma) were erupted. The rate of eruption was much lower between 14.9 and 14.0 Ma during the accumulation of tephras and distal ash-flow tuffs of the Tunnel Formation (Fig. 4a). During this early volcanism, magma erupted at a time-averaged rate of about 50 km^3/100 k.y. (Fig. 4b). At 14.0 Ma, metaluminous lava of Tram Ridge erupted from many centers, followed soon after by the related Lithic Ridge Tuff. Eruption of the peralkaline Grouse Canyon Tuff (13.7 Ma; Fig. 4a) caused the initial caldera collapse in the Silent Canyon caldera complex (Fig. 1), subsequently filled by lavas and tuffs of the peralkaline Dead Horse Flat Formation until 13.5 Ma. Between 14.0 and 12.8 Ma the rate of volcanic eruption increased to about 160 km^3/100 k.y. (Fig. 4b), and the greatest number of separate eruptive centers were active. Centers active during this time include the sources of the Crater Flat Group tuffs (ca. 13.25 Ma), the Wahmonie andesitic volcano (13.0 Ma; Fig. 4a), widespread Calico Hills lava vents (12.9 Ma), and Paintbrush Group calderas and lava vents. The peak of early SWNVF volcanism was eruption of Paintbrush Group tuffs and lavas, including the Topopah Spring Tuff (12.8 Ma) and Tiva Canyon Tuff (12.7 Ma), within 100 k.y. The rapid rate of magma extrusion, about 2250 km^3/100 k.y. (Table 1; Fig. 4b), was the highest during the lifetime of the SWNVF.

Lava flows that were petrographically similar to the Timber Mountain Group magma (for example, rhyolite of the Loop, Tables 1 and 3) were first erupted at ca. 12.5 Ma, but between 12.45 and 11.7 Ma no eruptions occurred (Fig. 4a) in the SWNVF. This 750 k.y. magma gap probably represents the time of magma generation and accumulation in magma chambers prior to the climactic eruption of the Timber Mountain Group tuffs. Precursory eruptions of rhyolite lava began ca. 11.7 Ma and were followed by the first of two major Timber Mountain Group ash-flow sheets, the Rainier Mesa Tuff, at 11.6 Ma. Rhyolite lava eruptions continued after eruption of the Rainier Mesa Tuff and preceded eruption of the second major Timber Mountain ash-flow sheet, the Ammonia Tanks Tuff, at 11.45 Ma. The Timber Mountain eruptions represent the second major peak of volcanism in the SWNVF, and time-averaged eruption rates on the order of 900 km^3/100 k.y. (Fig. 4b) characterized a 250 k.y. period. Significant basalt was first erupted in the SWNVF during Timber Mountain time. Ash flows and postcaldera moat lava flow eruptions related to the Ammonia Tanks Tuff followed soon after; rhyolite lava flows and tuffs erupted primarily west of the caldera.

Local rhyolite lava flows and more widespread basalt eruptions continued after 11.45 Ma during waning SWNVF volcanism. A 2 m.y. gap separates peak Timber Mountain ash-flow eruptions and the next caldera-forming eruptions of the Black Mountain caldera (Fig. 4a). Units of the peralkaline Thirsty Canyon Group, ash-flow sheets that total about 300 km^3 in volume, were erupted from the Black Mountain caldera after 9.4 Ma. The Stonewall Mountain caldera erupted almost 2 m.y. later than the Black Mountain caldera (Spearhead Member, 7.5 Ma). Eruption rates (15 km^3/100 k.y.) were low during this waning stage of SWNVF volcanism (Fig. 4b).

Episodic volcanic activity observed in the SWNVF is similar to some multicaldera Oligocene to Quaternary volcanic fields but contrasts with temporal patterns observed in others. The Mogollon-Datil volcanic field displays a similar episodicity in major caldera pulses (McIntosh and others, 1992), but caldera sources there had lateral migrations, which contrast with sequential eruptions from a single area of overlapping calderas in the SWNVF (Warren, 1983). The San Juan volcanic field, like the Mogollon-Datil, is composed of several overlapping clusters of calderas, each of which might be considered analogous to the SWNVF. $^{40}Ar/^{39}Ar$ geochronologic data for the central San Juan caldera cluster (Lanphere, 1988) indicate a peak volcanic eruption rate and frequency (the four middle, out of six, caldera eruptions were about 250 k.y. apart) comparable to the SWNVF. The waxing, waning, and eventual extinction of silicic volcanism in the SWNVF contrasts with the time-predictable migration of silicic volcanism along the Yellowstone–eastern Snake River Plain hot-spot track (Pierce and Morgan, 1992).

Magmatic Evolution of the SWNVF: The Relationship of Peralkaline and Metaluminous Volcanism in Time and Space

Magma composition varied along with eruptive volume during the lifetime of the SWNVF. Peralkaline magmas were erupted at several time intervals interspersed with eruption of the dominant metaluminous magmas, and source areas for the peralkaline magmas overlapped in part the metaluminous sources (Figs. 1 and 5a), in contrast to previous interpretations (Byers and others, 1976a; Christiansen and others, 1977; Noble and others, 1991). Earliest volcanism in the SWNVF produced mainly metaluminous ash-flow tuffs, including the Redrock Valley Tuff and the tuff of Yucca Flat; late in the earliest volcanic episode, however, peralkaline Tub Spring Tuff was erupted. Zirconium concentrations (Fig. 5a) are high in the peralkaline units, whereas modal plagioclase is very low to absent (Fig. 5b). Large-volume metaluminous volcanism began again at 14.0 Ma (Fig. 4a) with the eruption of the lava of Tram Ridge and the Lithic Ridge Tuff; these units have typical low zirconium contents and high modal plagioclase contents (Figs. 5a and 5b). Peralkaline comendite of Split Ridge lava, Grouse Canyon Tuff (the largest peralkaline ash-flow sheet in the SWNVF), and Dead Horse Flat lavas were erupted between 13.85 and 13.5 Ma.

The Grouse Canyon Tuff and lavas of the Dead Horse Flat Formation ponded in the northeastern caldera of the Silent Canyon caldera complex and were subsequently

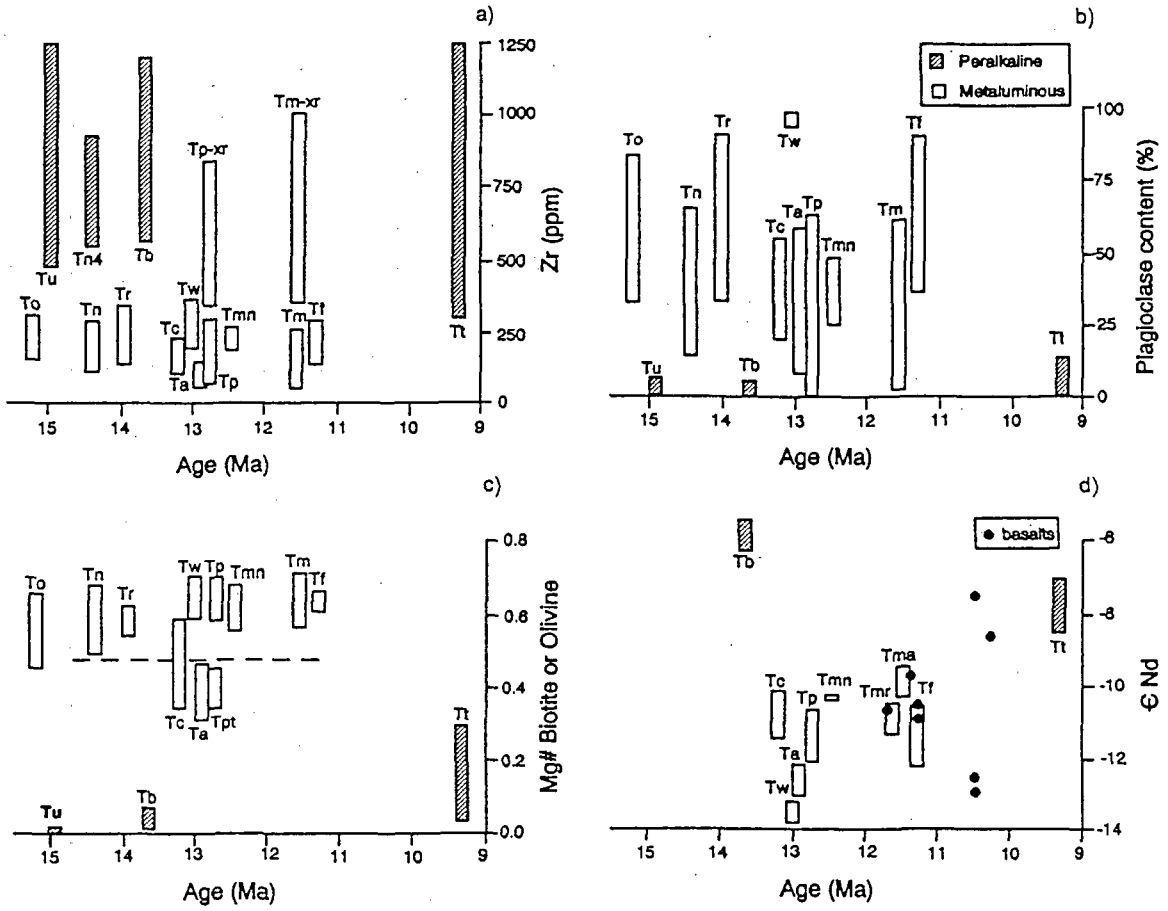

Figure 5. Ranges for selected chemical, petrographic, and isotopic characteristics of assemblages and units of the southwestern Nevada volcanic field (SWNVF) through time. (a) Ranges of zirconium contents for whole-rock samples. (b) Ranges of median proportions of plagioclase phenocrysts among felsic phenocrysts in units of each assemblage, as determined by petrography. (c) The variation of Mg# [Mg/(Mg + total Fe)] in biotite or olivine. (d) The range of analyzed neodymium isotopic compositions for each assemblage, coeval basalts, and selected units (Tegtmeyer, 1990; Tegtmeyer and Farmer, 1990; Farmer and others, 1991). Symbols from Table 1 except for Tm-xr, Timber Mountain Group, crystal-rich tops of ash-flow sheets; Tmn, transitional Timber Mountain Group lavas (Broxton and others, 1989); Tp-xr, Paintbrush Group, crystal-rich tops of ash-flow sheets; Tma, Ammonia Tanks Tuff; Tmr, Rainier Mesa Tuff; Tpt, Topopah Spring Tuff; and Tn4, Tunnel Formation subunit 4j. Hachured pattern for peralkaline units; metaluminous units unpatterned.

overlapped by the Area 20 caldera (Fig. 1). Metaluminous Bullfrog Tuff (13.25 Ma) of the Crater Flat Group and the postcaldera Calico Hills Formation lavas and tuffs (12.9 Ma) filled the Area 20 caldera (Warren, 1983). Peralkaline Belted Range Group and metaluminous Crater Flat Group and Calico Hills lavas have typical zirconium and plagioclase contents for their respective magma chemistries (Figs. 5a and 5b), but the mafic mineral chemistry of Crater Flat and Calico Hills units are anomalously iron-rich relative to other metaluminous rocks of the SWNVF (Fig. 5c). Iron enrichment (and corresponding magnesium depletion) of biotite and pyroxene in these metaluminous rocks is transitional to the extreme iron enrichment (Fig. 5c) characteristic of peralkaline mafic minerals (for example, fayalitic olivine and acmite). We interpret this pattern to indicate some degree of magmatic interaction, inheritance, or similarity in origin or evolution between the peralkaline Grouse Canyon magmatic system and the younger, spatially overlapping metaluminous Bullfrog Tuff and Calico Hills Formation magma systems. Iron-enriched mafic minerals also are present in the lower Topopah Spring Tuff (Tpt, Fig. 5c), suggesting a relationship between the Crater Flat/Calico Hills magmas and the initial Paintbrush Group magmas.

Magma chemistry of both Paintbrush and Timber Mountain caldera episodes is fundamentally metaluminous, although all four major ash-flow sheets are zoned from early-erupted high-silica rhyolite to late-erupted moderately alkalic trachytic compositions. Paintbrush Group rhyolites are slightly more alkalic than the Timber Mountain Group rhyolites. The higher zirconium contents of crystal-rich Paintbrush and Timber Mountain magmas (Fig. 5a) reflect accumulation of zircon included in cumulate phenocrysts (Warren and others, 1989) and are not due to high magmatic zirconium contents. Late peralkaline volcanism occurred with the eruption of the Thirsty Canyon Group magmas at 9.4 Ma (Figs. 5a, 5b, and 5c), after a 2 m.y. gap in ash-flow caldera-forming eruptions, during which time small-volume basalts and metaluminous rhyolites were erupted (Fig. 4a, and Tf, Figs. 5a, 5b, and 5c). Basaltic volcanism associated with the peralkaline Black Mountain caldera was more voluminous and widespread than with the two earlier peralkaline ash-flow tuffs. Peralkaline magmatism in the SWNVF occurred principally during the early (Tub Spring Tuff and Grouse Canyon Tuff), waxing phase of volcanism in the SWNVF, and during the late, waning stages of SWNVF activity at the Black Mountain

caldera (Vogel and others, 1983). Peralkaline SWNVF volcanism continued until the 7.5 Ma volcanism at the Stonewall Mountain volcanic center (Noble and others, 1984; Hausback and others, 1990).

The Nd isotopic composition of peralkaline magmas of the SWNVF is distinctive (Fig. 5d) with respect to metaluminous magmas (Tegtmeyer, 1990; Tegtmeyer and Farmer, 1990; Farmer and others, 1991). Peralkaline units have $\varepsilon Nd > -9$, whereas metaluminous units have $\varepsilon Nd < -9$. Metaluminous andesites of the Wahmonie volcano have the lowest εNd values (Farmer and others, 1991) in the SWNVF (Fig. 5d) and are petrographically distinguished by their high modal plagioclase contents (Fig. 5b) and calcic chemistry (Broxton and others, 1989). Spatially, the Wahmonie volcano is southeast of the central SWNVF caldera cluster (Fig. 1). These observations support a derivation of Wahmonie magmas from sources distinct from the rest of the SWNVF (Broxton and others, 1989).

Basaltic eruptions, starting in the metaluminous Timber Mountain episode and continuing through the eruption of peralkaline Thirsty Canyon tuffs, became more voluminous late in the history of the SWNVF (Figs. 4a and 5d). The Nd isotopic compositions of basalts and associated Timber Mountain Group tuffs and post–Timber Mountain rhyolite lavas are similar (Fig. 5d); most vents are south of the Silent Canyon caldera complex (Fig. 1). In contrast, younger basalts generally coeval with the peralkaline Thirsty Canyon tuffs were erupted mainly from volcanic centers on the north side of the SWNVF. Similarity of high values for εNd in young basalt and the peralkaline tuffs (Fig. 5d) and the geographic restriction of peralkaline sources to the northern SWNVF suggest that a lithospheric mantle boundary may exist between the Black Mountain and Grouse Canyon calderas to the north and the Timber Mountain caldera complex to the south.

Relation of Extension to SWNVF Volcanism

The relationship of Tertiary volcanism to extension in the Great Basin has been the subject of much controversy. Some have asserted that magmatism was prerequisite to large amounts of extension (Gans and others, 1989); others have found little evidence for significant extension during times of peak volcanism (Best and Christiansen, 1991). Extensional deformation in the SWNVF area (Figs. 1 and 6) variously preceded volcanism, was synchronous with volcanism in discrete domains, and postdated caldera volcanism. Probably most extensional deformation in the SWNVF area is middle to late Miocene (16–8 Ma) in age and thus coincides with the peak of extensional deformation (15–5 Ma) in the central Basin and Range of Wernicke (1992) to the south.

Prevolcanic extension is known to have affected several localities in the SWNVF area, but the timing and amount of this extension are difficult to determine because (1) the youngest affected units are Pennsylvanian, (2) structural reconstructions are complicated by Mesozoic thrust-faulting, and (3) exposures of pre-Tertiary rocks are limited (Fig. 6). Low-angle extensional faults cut Paleozoic and older sedimentary rocks around the margins of Yucca Flat (Fig. 6) at Mine Mountain (Hudson and Cole, 1993; Cole and others, 1989), the CP Hills (Caskey, 1991), and in the northern Halfpint Range (J. C. Cole, 1993, oral commun.; Barnes and others, 1963, 1965). Prevolcanic extension at Mine Mountain is older than the Redrock Valley Tuff (15.25 Ma) and younger than Mesozoic thrusting. Gently dipping 27.3 Ma Monotony Tuff and 26.7 Ma Shingle Pass Tuff (Sargent and Orkild, 1973; ages from Best and Christiansen, 1991) and conformable 14.9 Ma Tub Spring Tuff in the northern Halfpint Range depositionally overlie extended late Precambrian and Paleozoic rocks. On the northwest side of the Belted Range, 30°-dipping Monotony and Shingle Pass Tuffs overlie overturned Paleozoic rocks at Limestone Ridge that are cut by low-angle normal faults (Ekren and others, 1971). Thus, at least in the northern Halfpint and the Belted Ranges, early extensional deformation is pre–late Oligocene in age. Evidence from a drill hole at Rainier Mesa suggests that some prevolcanic extension may be pre–Late Cretaceous (Cole and others, 1993). We find no data that support postulated strong Paleogene extension (Axen and others, 1993) within the area of the central SWNVF caldera cluster (Fig. 6).

Synvolcanic normal faulting, minor strike-slip faulting, and tilting took place throughout the main period (14–11.5 Ma) of magmatism in the SWNVF (Fig. 4b), but extensional strain was modest in and near the central SWNVF caldera cluster (Fig. 6). Age constraints for this deformation come from overlap of faults in older units by younger units, from angular unconformities between units, and from thickness changes of units related to growth faulting. We describe below a composite pattern of synvolcanic and postvolcanic deformation (Fig. 4b), but with the following overall characteristics: (1) small cumulative middle to late Miocene extension of the central SWNVF relative to adjoining parts of the Great Basin (Hudson and others, 1994; Wernicke, 1992; Axen and others, 1993) and (2) greater extension in discrete domains (Fig. 6) marginal to the SWNVF at different specific times. These episodic extensional strains were distinctly nonuniform across the area of the SWNVF.

Early synvolcanic extension affected several localities of the SWNVF. Small strains were accommodated by pre-Bullfrog (13.25 Ma) normal faults and spatially limited pre–Tiva Canyon (12.7 Ma) normal and strike-slip faults northwest of Yucca Flat (Minor, 1989). Moderate pre-Bullfrog faulting and northwest tilting also affected an area southeast (Fig. 6) of Tolicha Peak (Minor and others, 1991, 1993). Large subsurface thickness changes of the lower Crater Flat Group tuffs and the Lithic Ridge Tuff reflect growth faulting at northern Yucca Mountain (Fridrich and others, 1994). Warren and others (1985) reported slight (2°–4°) pre–Timber Mountain northeast tilting of Paintbrush Group tuffs and lavas in the subsurface of Pahute Mesa. Calico Hills Formation and Paintbrush Group tuff thicken on the western, downthrown side of different faults at Pahute Mesa. Slight post-Paintbrush extension also occurred at Pahute Mesa where Rainier Mesa Tuff thickens over the same structures.

Late synvolcanic extensional deformation is greater in magnitude (Fig. 4b) on the southwestern margins of the SWNVF. In the Fluorspar Canyon area (Fig. 6), north of Bare Mountain (Monsen and others, 1992), the Bullfrog, Topopah Spring, and Tiva Canyon Tuffs are conformable and tilted east ~30°–60° more than the overlying 11.6–11.45 Ma Rainier Mesa and Ammonia Tanks Tuffs (discordant Timber Mountain tuffs of Carr, 1990, Fig. 4). At Yucca Mountain, Scott (1990) measured differential tilting of 10°–20° between Tiva Canyon Tuff and Timber Mountain Group tuffs at the south end of Yucca Mountain; the Tiva Canyon Tuff was rotated ~25° clockwise about a vertical axis, whereas rotation of the Ammonia Tanks Tuff (6° ± 13°) was much less (Rosenbaum and others, 1991; Hudson and others, 1994).

Postvolcanic extension (defined as younger than the 11.45 Ma Ammonia Tanks Tuff, Fig. 4b) was locally large in magnitude but was restricted to areas marginal to the central SWNVF caldera cluster (Fig. 6). Moderate to large postvolcanic extension occurred in the Bullfrog Hills and Fluorspar Canyon areas (Fig. 6). Extension was ex-

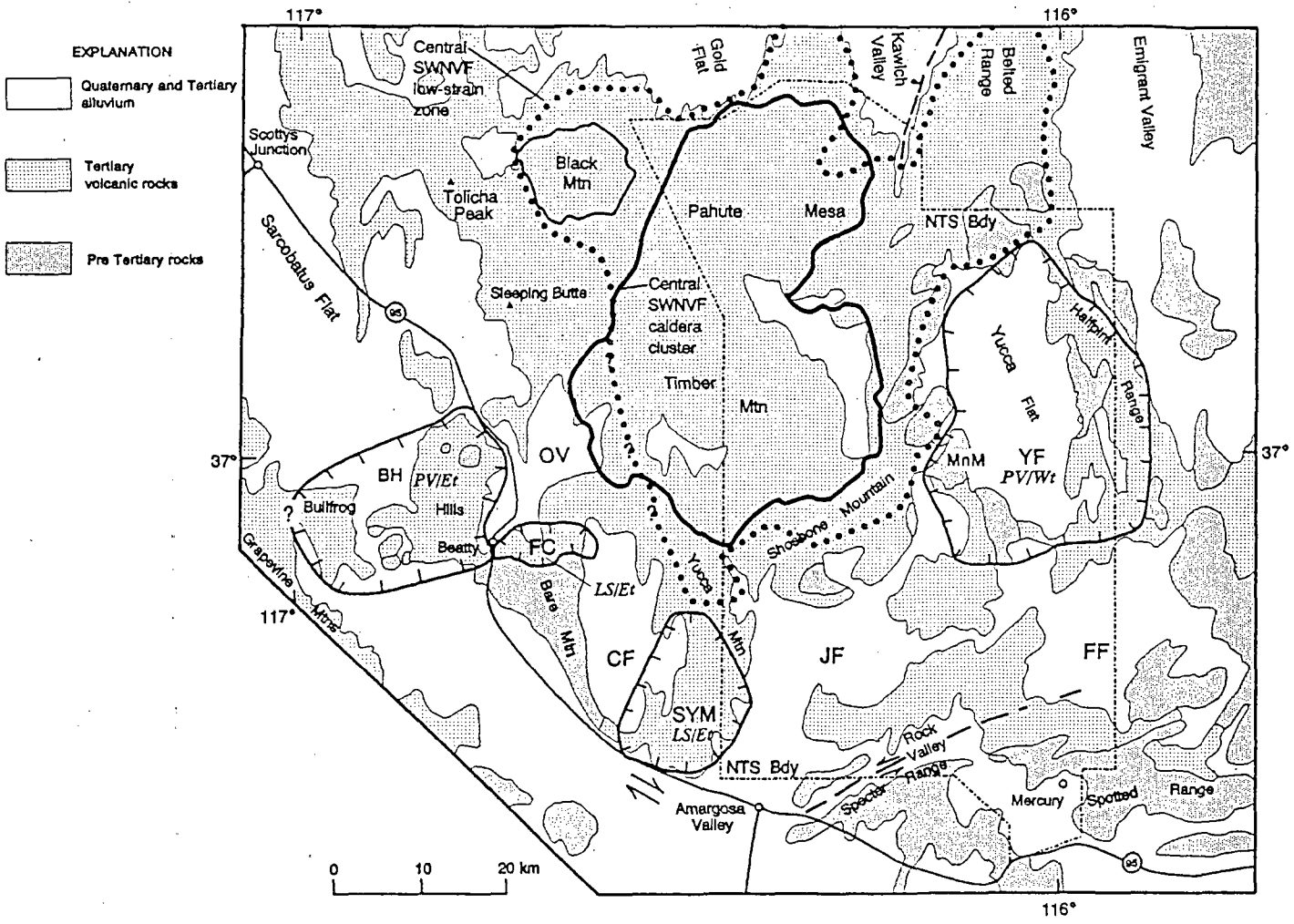

Figure 6. Map illustrating the central southwestern Nevada volcanic field (SWNVF) caldera cluster and outlining the area showing weak (<10° of tilt or vertical-axis rotation) syn- and postvolcanic deformation, and some marginal domains (enclosed by hachured lines) of moderate to large amounts of late synvolcanic (*LS*) and postvolcanic (*PV*) extension. Tilt direction of beds is indicated by *Et*, east tilt, and *Wt*, west tilt. Abbreviations for labeled domains are from Figure 4b. Additional postvolcanic domains of moderate extension that formed alluvial basins include OV, Oasis Valley; CF, Crater Flat; JF, Jackass Flats; FF, Frenchman Flat; but boundaries for these domains are not completely delimited at present. The area of prevolcanic extension at Mine Mountain is abbreviated as MnM; Nevada Test Site is abbreviated as NTS. The map is not a comprehensive depiction of all synvolcanic and postvolcanic extensional domains in the SWNVF but represents the domains that can be identified at present, relative to the central SWNVF low-strain zone.

treme in the Bullfrog Hills, where 60°–90° east tilts are observed in conformable sequences ranging from pre–Lithic Ridge Tuff to the Ammonia Tanks Tuff (Maldonado, 1990), but largely predated 10 Ma latite flows (Maldonado and Hausback, 1990). In the western Fluorspar Canyon area (Monsen and others, 1992), Ammonia Tanks Tuff is tilted east as much as 30°. Farther east in Crater Flat, across Yucca Mountain, and southeast of Timber Mountain, the Timber Mountain Group tuffs are generally tilted 10°–30° (Carr, 1990, Fig. 4). Postvolcanic extension was minimal at Pahute Mesa, where Timber Mountain tuffs tilt east <4° (Warren and others, 1985). Slight normal faulting there (offsets >60–80 m on principal faults) and slight (<2°) tilting affected the 9.4 Ma Thirsty Canyon Group (Orkild and others, 1969).

Fault-controlled, post–Ammonia Tanks alluvial sedimentary basins formed on the margins of the SWNVF but do not overlap the central SWNVF caldera cluster. The Yucca Flat basin–Halfpint Range fault system, east of the central SWNVF, is a post–Ammonia Tanks alluvial basin filled by late Miocene and younger sedimentary deposits (Barnes and others, 1963) to 400 m depth, and locally as much as 1200 m (McKeown and others, 1976). In Yucca Flat (Fig. 6) and the Halfpint Range, units of the SWNVF are cut by similar down-to-the-east normal faults and exhibit stratal tilts of 10°–25° west (Frizzell and Shulters, 1990, and sources cited therein). Similar alluvial basins of late Miocene to Quaternary age are present north (Gold Flat, Kawich Valley, and Emigrant Valley) and south (Crater Flat, Jackass Flat, and Frenchman Flat) of the central SWNVF (Fig. 6), but their controlling faults did not propagate across the area of peak volcanism and caldera formation. The central SWNVF is one of the largest areas in the Great Basin unbroken by middle Miocene and younger alluvial basins (Stewart and Carlson, 1978); the northern Basin and Range pattern of paired late Neogene north-south ranges and basins terminates at the north margin of SWNVF. Rainier Mesa Tuff is repeated in fault blocks at about the

same elevation over an east-west distance of 100 km, from the Bullfrog Hills to the Halfpint Range, with no headwall breakaway zones or regions of uplifted lower plate rocks (W. B. Hamilton, 1993, written commun.).

Volcanism and extension that postdate the central SWNVF have different patterns in time and space. Christiansen and Lipman (1972) suggested that extension and volcanism in the SWNVF area occurred after a transition from magmatism generated by subduction to a regime characterized by extension and bimodal basalt-rhyolite volcanism. Magmatism and extension in the SWNVF area also occurred as the Mendocino fracture zone migrated north as a locus for magmatism and extension (Glazner and Bartley, 1984). Detailed plate tectonic reconstructions (Severinghaus and Atwater, 1990) indicate that during the main episode of volcanism (14–11.5 Ma) the SWNVF was located north of the Mendocino fracture zone. In the SWNVF area at this time, the Pacific plate was still being subducted beneath an extending western North America, analogous to the Lassen–Shasta–Medicine Lake Highlands region of northern California today. Younger SWNVF calderas (Black Mountain, 9.4 Ma, and Stonewall Mountain, 7.5 Ma) were peralkaline in composition and small in volume (Fig. 4b), and they migrated northwestward, consistent with a melting locus associated with the movement of the Mendocino fracture zone. Late Miocene and Pliocene silicic caldera volcanism in the southern Great Basin (6 Ma Silver Peak volcanic center) migrated west-northwest toward the Pliocene and Quaternary Long Valley–Mono Basin volcanic system (Luedke and Smith, 1981), whereas younger extension and strike-slip faulting migrated west toward the Death Valley region (Hamilton, 1988).

In contrast to models by Gans and others (1989), we find that the area of greatest magma input to upper crust—within the overlapping Silent Canyon–Claim Canyon–Timber Mountain caldera complexes (Fig. 6)—is the area of least upper crustal extension. Several factors may have led to retardation of extension in the area of the central SWNVF caldera cluster. The caldera complexes are probably rooted in batholith cupolas (Lipman, 1984). After crystallization and cooling, such batholiths could act as buttresses (Wernicke, 1992; Hamilton and Myers, 1966), strengthening the upper crust against regional extensional stress. Crustal strengthening probably best explains retardation of postvolcanic (post–Ammonia Tanks Tuff) extension in the central SWNVF. A strengthening of the crust during synvolcanic extension, however, would require that magmas were emplaced and cooled quickly relative to deformation. This might be possible at shallow crustal levels, as described by Davis and others (1993) for a pluton that intruded and terminated slip on a coeval Miocene detachment fault in the eastern Mojave Desert. For synvolcanic extension, silicic magma input and inflation of the batholithic magma chamber roof also may have affected the regional stress field, reducing the regional deviatoric stress (Parsons and Thompson, 1991) and decreasing regional strain. Quaternary volcanic fields that exhibit similar deformational patterns include the Yellowstone Plateau volcanic field, where neotectonic late Pleistocene and Holocene regional normal faults splay, decrease in displacement, and terminate to the north approaching the 0.6 Ma third-cycle Yellowstone caldera (Pierce and Morgan, 1992, Plate 1), and the Long Valley–Mono Basin volcanic system (Bursik and Sieh, 1989; Dixon and others, 1993).

Miocene extension in the SWNVF occurred in a mosaic of local domains. South and west margins of the field were affected by a dextral shear transfer zone (Rosenbaum and others, 1991; Hudson and others, 1994) that is a northern boundary for the high-strain Death Valley extensional corridor (Wernicke and others, 1988). In general, SWNVF volcanism and regional extension were coeval. In detail, however, age, magnitude, and polarity of extension varied among the more strongly deformed domains marginal to the field. Both volcanism and extensional deformation in the SWNVF were episodic in nature as has been recognized in the eastern Great Basin (Taylor and others, 1989).

SUMMARY

Volcanic activity in the SWNVF, as revealed by new high-resolution $^{40}Ar/^{39}Ar$ age determinations, was distinctly episodic: very large volumes of magma (up to 2000 km^3) were erupted in fairly short periods of <100–300 k.y. separated by longer quiescent periods. For example, two episodes of caldera-forming ash-flow magmatism, separated by a 750 k.y. magma gap, produced the large-volume tuffs of the Paintbrush and Timber Mountain Groups during a 1.35 m.y. time period. New $^{40}Ar/^{39}Ar$ ages corroborate the stratigraphic succession of units within the SWNVF based upon petrographic, geochemical, and field geologic studies (Byers and others, 1976a; Warren and others, 1988; Broxton and others, 1989; Sawyer and Sargent, 1989; Minor and others, 1993). We have revised the stratigraphy of major SWNVF units based upon this new framework, combining major ash-flow sheets with petrologically related lava flows and nonwelded tuff deposits into stratigraphic groups. Newly defined formal stratigraphic units are the Beatty Wash Formation, Calico Hills Formation, Dead Horse Flat Formation, and Tunnel Formation. The revised stratigraphy and ages demonstrate that peralkaline volcanism in the SWNVF was closely associated in time and space with the waxing and waning of metaluminous volcanism. Petrologic and chemical data provide evidence of hybridization between distinct peralkaline and metaluminous magmas during the 7 m.y. span of SWNVF volcanism.

Minor to moderate extension can be demonstrated during the history of the SWNVF, but the slight synvolcanic extension of the central SWNVF contrasts markedly with the synextensional magmatism described by Gans and others (1989) for limited areas of highly extended volcanic rocks in the Great Basin. Best and Christiansen (1991) concluded that the Oligocene and early Miocene peak of volcanism in the Great Basin correlated with only limited extension in east-central Nevada. For the SWNVF, we extend their conclusions in that only limited extension occurred during peak middle Miocene volcanism in the southwestern Great Basin. Within the SWNVF, the central area of coalescing calderas and proximal caldera margins was minimally extended from middle Miocene to the present. Synvolcanic strain was dominated by local magma chamber roof deformation or caldera subsidence (Lipman, 1984). The outer margins of the SWNVF locally were more deformed in discrete extensional domains. An inferred subcaldera batholith may have acted as an upper crustal buttress with respect to regional extensional deformation. Intense middle Miocene volcanism and subjacent plutonism apparently strengthened the upper crust in the central SWNVF area, because it stands today as a high plateau unbroken by regional middle Miocene and younger normal faulting that formed young alluvial basins. Magmatism in the SWNVF and regional extension, although coeval, were not genetically linked to form a zone of highly extended upper crust. The two processes

overlapped in time and space but were not correlated in amount.

ACKNOWLEDGMENTS

J. C. Cole, P. P. Orkild, and G. A. Izett provided encouragement and guidance in the formulation of the study. We thank G. B. Dalrymple for the opportunity to work on the "GLM" at the U.S. Geological Survey in Menlo Park. The support of Gerry Cebula and Jack Groen for superb mineral separations; of James Saburomaru, Jerry von Essen, and Malcolm Pringle in the lab; of Ray Sabala for scientific illustrations; and from H. Dickensheets, R. Durham, and D. Welch of the U.S. Air Force in providing access is gratefully acknowledged.

Review comments by V. M. Glanzman, W. D. Johnson Jr., P. P. Orkild, Marge MacLachlan, Tom Judkins, Dave Schleicher, Ed du Bray, W. J. Carr, F. M. Byers Jr., J. C. Cole, S. A. Minor, C. J. Fridrich, C. M. Johnson, W. McIntosh, S. Mertzman, A. G. Sylvester, and J. R. LeCompte helped correct many errors of commission and omission; however, the conclusions and any remaining errors remain the responsibility of the authors. This project was funded under Interagency Agreement DE-AI08-91NV11040 between the U.S. Geological Survey and the Department of Energy, Nevada Operations Office.

APPENDIX: ANALYTICAL METHODS

Sanidine separates for this study were prepared by Kistler (1968), Marvin and others (1970, 1973, 1989), Marvin and Cole (1978), and Fred McDowell (University of Texas, 1989, written commun.) and were previously analyzed by the conventional K/Ar method, were new sanidine separates prepared at Los Alamos National Laboratory, or were new sanidine and biotite prepared at the U.S. Geological Survey (USGS) mineral separation facility in Denver, Colorado. Sanidine separates were leached with dilute HF followed by ultrasonic cleaning to remove volcanic glass and other surface impurities. Only a few milligrams of sanidine were encapsulated in aluminum foil for irradiation; biotite samples for incremental heating weighed about 100 mg. The sanidine and biotite capsules were placed in fused silica vials with flux monitor standards (Taylor Creek Rhyolite sanidine, Fish Canyon Tuff sanidine, and SB-3 biotite) placed at regular intervals and were irradiated in the USGS TRIGA reactor in Denver, Colorado, using the procedures described in Dalrymple and others (1981) over the course of four irradiations (LXXXIV, LXXXVII, XCIII, and CII) between 1989 and 1991; all pooled results of multiple samples are from the first two irradiations. Typical irradiation time was 16 hr and resulted in total neutron doses of about 1×10^{18} nvt (nvt = neutron density × neutron velocity × irradiation time).

Dalrymple and Duffield (1988) and Dalrymple (1989) described the analytical capabilities of the 5W Ar-ion continuous laser $^{40}Ar/^{39}Ar$ laboratory in Menlo Park. Analysis of sanidine generally involved fusing 6–8 grains of sanidine; in a few cases up to 15 grains of finer-size sanidine (<100 mesh) were fused, and for several samples large single crystals were analyzed. Approximate masses of sanidine fused in each analysis were 0.005–0.4 mg. Typically, each age determination represents the weighted mean of 4–6 sanidine laser-fusion analyses (Table 3). Mass analyses were performed on a MAP 216 mass spectrometer at a sensitivity of about 2×10^{-14} mol/V. The incremental heating/age spectrum $^{40}Ar/^{39}Ar$ technique (Dalrymple and Lanphere, 1971; Lanphere, 1988) was used to degas ~100 mg biotite samples in a resistance-heated furnace in 8–12 temperature increments; temperatures were measured using a thermocouple. Argon isotopic ratios were measured on a 6 in. (15.2 cm) radius, 60° sector, Nier-type single-collector mass spectrometer. Corrections for undesirable interferences of ^{36}Ar, ^{39}Ar, and ^{40}Ar isotopes caused by nuclear reactions of K and Ca were made using standard calculations (Dalrymple and others, 1981). All $^{40}Ar/^{39}Ar$ ages have been measured relative to a monitor age of 513.9 Ma for MMhb-1 (Lanphere and others, 1990; Dalrymple and others, 1993). An age of 27.92 Ma was calculated for the internal monitor standard Taylor Creek Rhyolite sanidine 85G003.

Uncertainties in weighted means are the inverse variance-weighted 1σ standard error of the mean (Taylor, 1982) for multiple laser fusion analyses or fractions of an incremental-heating age spectrum and include propagation of the J-curve calibration uncertainty. Pooled ages for multiple samples of a unit are weighted means of several determinations. Estimates of errors assigned to individual age measurements (internal errors) are made by propagating well-documented errors from all aspects of each analysis (Cox and Dalrymple, 1967; Taylor, 1982). Reproducibility of ages (external error) in highly radiogenic samples such as sanidine and biotite is generally as good or better than internal errors unless geologic factors such as contamination or argon loss are present. The cited best estimate uncertainty of the weighted mean is the square root of the sum of the weighting factors (Taylor, 1982) and represents a 1σ (68.27%) confidence interval of the mean. These uncertainties are analogous to the standard error of the mean (s.e.m., Table 3) for arithmetic means except that they only include internal errors and thus do not include excess dispersion of the measured ages. External error in excess of the internal estimates is alternatively incorporated using the mean square of weighted deviates (MSWD, McIntyre and others, 1966) as a measure of dispersion. Where MSWD is >1.0, estimated uncertainties are adjusted to incorporate the external error component, multiplying them by the square root of MSWD (Ludwig, 1988). Resulting uncertainties produce a MSWD of 1.0, maintaining the weighted mean and relative magnitudes of the error estimates for individual samples.

REFERENCES CITED

Axen, G. J., Taylor, W. J., and Bartley, J. M., 1993, Space-time patterns and tectonic controls of Tertiary extension and magmatism in the Great Basin of the western United States: Geological Society of America Bulletin, v. 105, p. 56–76.

Barnes, H., Houser, F. N., and Poole, F. G., 1963, Geologic map of the Oak Spring quadrangle: U.S. Geological Survey Map GQ-214, scale 1:24 000.

Barnes, H., Christiansen, R. L., and Byers, F. M., Jr., 1965, Geologic map of the Jangle Ridge quadrangle: U.S. Geological Survey Map GQ-363, scale 1:24 000.

Bath, G. D., 1968, Aeromagnetic anomalies related to remanent magnetism in volcanic rock, Nevada Test Site, *in* Eckel, E. B., ed., Nevada Test Site: Geological Society of America Memoir 110, p. 135–146.

Best, M. G., and Christiansen, E. H., 1991, Limited extension during peak Tertiary volcanism, Great Basin of Nevada and Utah: Journal of Geophysical Research, v. 96, no. N8, p. 13 509–13 528.

Broxton, D. E., Warren, R. G., Byers, F. M., Jr., and Scott, R. B., 1989, Chemical and mineralogical trends within the Timber Mountain–Oasis Valley caldera complex—Evidence for multiple cycles of chemical evolution in a long-lived silicic magma system: Journal of Geophysical Research, v. 94, p. 5961–5986.

Broxton, D. E., Chipera, S. J., Byers, F. M., Jr., and Rautman, C. A., 1993, Geologic evaluation of six nonwelded tuff sites in the vicinity of Yucca Mountain, Nevada for a surface-based test facility for the Yucca Mountain Project: Los Alamos National Laboratory Report LA-12542-MS, 83 p.

Bursik, M., and Sieh, K., 1989, Range front faulting and volcanism in the Mono Basin, eastern California: Journal of Geophysical Research, v. 94, p. 15 587–15 609.

Byers, F. M., Jr., Carr, W. J., Orkild, P. P., Quinlivan, W. D., and Sargent, K. A., 1976a, Volcanic suites and related cauldrons of Timber Mountain–Oasis Valley caldera complex, southern Nevada: U.S. Geological Survey Professional Paper 919, 70 p.

Byers, F. M., Jr., Carr, W. J., Orkild, P. P., Quinlivan, W. D., and Sargent, K. A., 1976b, Geologic map of the Timber Mountain caldera area: U.S. Geological Survey Miscellaneous Investigation Series Map I-891, scale 1:48 000.

Byers, F. M., Jr., Carr, W. J., and Orkild, P. P., 1989, Volcanic centers of southwestern Nevada—Evolution of understanding, 1960–1988: Journal of Geophysical Research, v. 94, p. 5908–5924.

Carr, W. J., 1990, Styles of extension in the Nevada Test Site region, southern Walker Lane belt—An integration of volcano-tectonic and detachment fault models, *in* Wernicke, B. P., ed., Basin and Range extensional tectonics near the latitude of Las Vegas, Nevada: Geological Society of America Memoir 176, p. 283–304.

Carr, W. J., Byers, F. M., Jr., and Orkild, P. P., 1986, Stratigraphic and volcano-tectonic relations of the Crater Flat Tuff and some older volcanic units: U.S. Geological Survey Professional Paper 1323, 28 p.

Caskey, S. J., 1991, Mesozoic and Cenozoic structural geology of the CP Hills, Nevada Test Site, Nye County, Nevada—And regional implications [M.S. thesis]: Reno, University of Nevada, 90 p.

Christiansen, R. L., 1979, Cooling units and composite sheets in relation to caldera structure, *in* Chapin, C. E., and Elston, W. E., eds., Ash-flow tuffs: Geological Society of America Memoir 180, p. 29–42.

Christiansen, R. L., and Lipman, P. W., 1965, Geologic map of the Topopah Spring Northwest quadrangle, Nye County, Nevada: U.S. Geological Survey Geologic Quadrangle Map GQ-444, scale 1:24 000.

Christiansen, R. L., and Lipman, P. W., 1972, Cenozoic volcanism and plate tectonic evolution of the Western United States—Part 2, Late Cenozoic: Royal Society of London Philosophical Transactions, ser. A, v. 271, p. 249–284.

Christiansen, R. L., Lipman, P. W., Carr, W. J., Byers, F. M., Jr., Orkild, P. P., and Sargent, K. A., 1977, The Timber Mountain–Oasis Valley caldera complex of southern Nevada: Geological Society of America Bulletin, v. 88, p. 943–959.

Cole, J. C., Wahl, R. R., and Hudson, M. R., 1989, Structural relations within the Paleozoic basement of the Mine Mountain block: Implications for interpretation of gravity data in Yucca Flat, Nevada Test Site, *in* Olsen, C. W., and Carter, J. A., eds., Proceedings, Fifth Symposium on Containment of Underground Nuclear Explosions: Lawrence Livermore National Laboratory Report CONF-8909163, v. 2, p. 431–455.

Cole, J. C., Harris, A. G., Lanphere, M. A., Barker, C. E., and Warren, R. G., 1993, The case for pre-middle Cretaceous extensional faulting in northern Yucca Flat, southwestern Nevada: Geological Society of America Abstracts with Programs, v. 25, no. 5, p. 22.

Cox, A., and Dalrymple, G. B., 1967, Statistical analysis of geomagnetic reversal data and the precision of potassium-argon dating: Journal of Geophysical Research, v. 72, p. 2603–2614.

Dalrymple, G. B., 1989, The GLM continuous laser system for $^{40}Ar/^{39}Ar$ dating: Description and performance characteristics: U.S. Geological Survey Bulletin 1890, p. 89–96.

Dalrymple, G. B., and Duffield, W. A., 1988, High precision $^{40}Ar/^{39}Ar$ dating of Oligocene rhyolites from the Mogollon-Datil volcanic field using a continuous laser system: Geophysical Research Letters, v. 15, p. 463–466.

Dalrymple, G. B., and Lanphere, M. A., 1971, $^{40}Ar/^{39}Ar$ technique of K-Ar dating—A comparison with the conventional technique: Earth and Planetary Science Letters, v. 12, p. 300–308.

Dalrymple, G. B., Alexander, E. C., Lanphere, M. A., and Kraker,

G. P., 1981, Irradiation of samples for $^{40}Ar/^{39}Ar$ dating using the Geological Survey TRIGA reactor: U.S. Geological Survey Professional Paper 1176, 55 p.

Dalrymple, G. B., Izett, G. A., Snee, L. W., and Obradovich, J. D., 1993, $^{40}Ar/^{39}Ar$ age spectra and total-fusion ages of tektites from Cretaceous-Tertiary rocks in the Beloc Formation, Haiti: U.S. Geological Survey Bulletin 2065, 20 p.

Davis, G. A., Fowler, T. K., Bishop, K. M., Brudos, T. C., Friedmann, S. J., Burbank, D. W., Parke, M. A., and Burchfiel, B. C., 1993, Pluton pinning of an active Miocene detachment fault system, eastern Mojave Desert, California: Geology, v. 21, p. 627–630.

Dixon, T. H., Bursik, M., Wolf, S. K., Hetlin, M., Webb, F., Farina, F., and Robaudo, S., 1993, Constraints on deformation of the resurgent dome, Long Valley caldera, California from Space Geodesy, *in* Smith, D. E., and Turcotte, D. L., eds., Contribution of Space Geodesy to geodynamics—Crustal dynamics: American Geophysical Union Geodynamics Series, v. 23, p. 193–214.

Ekren, E. B., Anderson, R. E., Rogers, C. L., and Noble, D. C., 1971, Geology of northern Nellis Air Force Base Bombing and Gunnery Range: U.S. Geological Survey Professional Paper 651, 91 p., scale 1:125 000.

Farmer, G. L., Broxton, D. E., Warren, R. G., and Pickthorn, William, 1991, Nd, Sr, and O isotopic variations in metaluminous ash-flow tuffs and related volcanic rocks at the Timber Mountain/Oasis Valley caldera complex, SW Nevada—Implications for the origin and evolution of large-volume silicic magma bodies: Contributions to Mineralogy and Petrology, v. 109, p. 53–68.

Ferguson, J. F., Cogbill, A. H., and Warren, R. G., 1994, A geophysical-geological transect of the Silent Canyon caldera complex, Pahute Mesa, Nevada: Journal of Geophysical Research, v. 99, p. 4323–4339.

Fridrich, C. J., Dudley, W. W., Jr., and Stuckless, J. S., 1994, A hydrogeologic analysis of the saturated zone ground-water system under Yucca Mountain, Nevada: Journal of Hydrology, v. 154, p. 133–168.

Frizzell, V. A., and Shulters, J., 1990, Geologic map of the Nevada Test Site, southern Nevada: U.S. Geological Survey Miscellaneous Investigations Series Map I-2046, scale 1:100 000.

Gans, P. B., Mahood, G. A., and Schermer, E., 1989, Synextensional magmatism in the Basin and Range province—A case study from the eastern Great Basin: Geological Society of America Special Paper 233, 53 p.

Gibbons, A. B., Hinrichs, E. N., Hansen, W. R., and Lemke, R. W., 1963, Geology of the Rainier Mesa quadrangle, Nye County, Nevada: U.S. Geological Survey Geologic Quadrangle Map GQ-215, scale 1:24 000.

Glazner, A. F., and Bartley, J. M., 1984, Timing and tectonic setting of Tertiary low-angle normal faulting and associated magmatism in the southwestern United States: Tectonics, v. 3, p. 385–396.

Hamilton, W. B., 1988, Detachment faulting in the Death Valley region, California and Nevada: U.S. Geological Survey Bulletin 1790, p. 51–85.

Hamilton, W. B., and Myers, W. B., 1966, Cenozoic tectonics of the western United States: Reviews of Geophysics, v. 4, p. 509–549.

Hansen, W. R., Lemke, R. W., Cattermole, J. M., and Gibbons, A. B., 1963, Stratigraphy and structure of the Rainier and USGS tunnel areas: U.S. Geological Survey Professional Paper 382-A, 49 p., scale 1:6000.

Hausback, B. P., Deino, A. L., Turrin, B. T., McKee, E. H., Frizzell, V. A., Jr., Noble, D. C., and Weiss, S. I., 1990, New $^{40}Ar/^{39}Ar$ ages for the Spearhead and Civet Cat Canyon Members of the Stonewall Flat Tuff, Nye County, Nevada—Evidence for systematic errors in standard K-Ar determinations on sanidine: Isochron/West, no. 56, p. 3–7.

Healey, D. L., 1968, Application of gravity data to geologic problems at Nevada Test Site, *in* Eckel, E. B., ed., Nevada Test Site: Geological Society of America Memoir 110, p. 147–156.

Healey, D. L., Harris, R. N., Ponce, D. A., and Oliver, H. W., 1987, Complete Bouger gravity map of the Nevada Test Site and vicinity, Nevada: U.S. Geological Survey Open-File Report 87-506, scale 1:100 000.

Hudson, M. R., and Cole, J. C., 1993, Kinematics of faulting in the Mine Mountain area of southern Nevada: Evidence for pre-middle Miocene extension: Geological Society of America Abstracts with Programs, v. 25, no. 5, p. 55.

Hudson, M. R., Sawyer, D. A., and Warren, D. A., 1994, Paleomagnetism and rotation constraints for the middle Miocene southwestern Nevada volcanic field: Tectonics, v. 13, p. 258–277.

Kane, M. F., Webring, M. W., and Bhattacharyya, B. K., 1981, A preliminary analysis of gravity and aeromagnetic surveys of the Timber Mountain area, southern Nevada: U.S. Geological Survey Open-File Report 81-189, 40 p., scale 1:48 000.

Kistler, R. W., 1968, Potassium-argon ages of volcanic rocks in Nye and Esmeralda counties, Nevada, *in* Eckel, E. B., ed., Nevada Test Site: Geological Society of America Memoir 110, p. 252–262.

Lanphere, M. A., 1988, High-resolution $^{40}Ar/^{39}Ar$ chronology of Oligocene volcanic rocks, San Juan Mountains, Colorado: Geochimica et Cosmochimica Acta, v. 52, p. 1425–1434.

Lanphere, M. A., Dalrymple, G. B., Fleck, R. J., and Pringle, M. S., 1990, Intercalibration of mineral standards for K-Ar and $^{40}Ar/^{39}Ar$ age measurements [abs.]: Eos (Transactions, American Geophysical Union), v. 71, p. 1658.

Lipman, P. W., 1984, Roots of ash-flow calderas—Windows into granitic batholiths: Journal of Geophysical Research, v. 89, p. 8801–8841.

Ludwig, K. R., 1988, ISOPLOT for MS-DOS, A plotting and regression program for radiogenic-isotope data, for IBM-PC compatible computers, v. 1.00: U.S. Geological Survey Open-File Report 88-557, 44 p.

Luedke, R. G., and Smith, R. L., 1981, Map showing distribution, composition, and age of late Cenozoic volcanic centers in California and Nevada: U.S. Geological Survey Miscellaneous Investigations Map I-1091-C, scale 1:1 000 000.

Maldonado, F., 1990, Structural geology of the upper plate of the Bullfrog Hills detachment system: Geological Society of America Bulletin, v. 102, p. 992–1006.

Maldonado, F., and Hausback, B. P., 1990, Geologic map of the northeast quarter of the Bullfrog 15-minute quadrangle, Nye County, Nevada: U.S. Geological Survey Miscellaneous Investigations Series Map I-2049, scale 1:24 000.

Marvin, R. F., and Cole, J. C., 1978, Radiometric ages—Compilation "A," U.S. Geological Survey: Isochron West, no. 22, p. 3–14.

Marvin, R. F., Byers, F. M., Jr., Mehnert, H. H., Orkild, P. P., and Stern, T. W., 1970, Radiometric ages and stratigraphic sequence of volcanic and plutonic rocks, southern Nye and western Lincoln Counties, Nevada: Geological Society of America Bulletin, v. 81, p. 2657–2676.

Marvin, R. F., Mehnert, H. H., and McKee, E. H., 1973, A summary of radiometric ages of Tertiary volcanic rocks in Nevada and eastern California, Part III—Southeastern Nevada: Isochron/West, no. 6, p. 1–30.

Marvin, R. F., Mehnert, H. H., and Naeser, C. W., 1989, U.S. Geological Survey radiometric ages—Compilation "C," Part three—California and Nevada: Isochron/West, no. 52, p. 3–11.

McDowell, F. W., 1983, K-Ar dating—Incomplete extraction of radiogenic argon from alkali feldspar: Isotope Geoscience, v. 1, p. 119–126.

McIntosh, W. C., Chapin, C. E., Ratte, J. C., and Sutter, J. F., 1992, Time-stratigraphic framework for the Eocene-Oligocene Mogollon-Datil volcanic field, southwest New Mexico: Geological Society of America Bulletin, v. 104, p. 851–871.

McIntyre, G. A., Brooks, C., Compston, W., and Turek, A., 1966, The statistical assessment of Rb-Sr isochrons: Journal of Geophysical Research, v. 71, p. 5459–5468.

McKeown, F. A., Healey, D. L., and Miller, C. H., 1976, Geologic map of the Yucca Lake quadrangle: U.S. Geological Survey Geologic Quadrangle Map GQ-1327, scale 1:24 000.

Minor, S. A., 1989, Paleostress investigation near Rainier Mesa, Nevada Test Site, *in* Olsen, C. W., and Carter, J. A., eds., Proceedings, Fifth Symposium on Containment of Underground Nuclear Explosions: Lawrence Livermore National Laboratory Report CONF-8909163, v. 2, p. 457–482.

Minor, S. A., Sawyer, D. A., Orkild, P. P., Coe, J. A., Wahl, R. R., and Frizzell, V. A., 1991, Neogene migratory extensional deformation revealed on new map of the Pahute Mesa 1:100,000-scale quadrangle, southern Nevada [abs.]: Eos (Transactions, American Geophysical Union), v. 72, p. 469.

Minor, S. A., Sawyer, D. A., Wahl, R. R., Frizzell, V. A., Schilling, S. P., Warren, R. G., Orkild, P. P., Coe, J. A., Hudson, M. R., Fleck, R. J., Lanphere, M. A., Swadley, W. C., and Cole, J. C., 1993, Preliminary geologic map of the Pahute Mesa 30′ × 60′ quadrangle: U.S. Geological Survey Open-File Report 93-299, 39 p., scale 1:100 000.

Monsen, S. A., Carr, M. D., Reheis, M. C., and Orkild, P. P., 1992, Geologic map of Bare Mountain, Nye County, Nevada: U.S. Geological Survey Miscellaneous Investigations Map I-2201, scale 1:24 000.

Noble, D. C., Vogel, T. A., Weiss, S. I., Erwin, J. W., McKee, E. H., and Younker, L. W., 1984, Stratigraphic relations and source areas of ash flow sheets of the Black Mountain and Stonewall volcanic centers, Nevada: Journal of Geophysical Research, v. 89, p. 8593–8602.

Noble, D. C., Weiss, S. I., and McKee, E. H., 1991, Magmatic and hydrothermal activity, caldera geology, and regional extension in the western part of the southwestern Nevada volcanic field, *in* Raines, G. L., Lisle, R. E., Schaefer, R. W., and Wilkinson, W. H., eds., Geology and ore deposits of the Great Basin, Symposium Proceedings: Reno, Geological Society of Nevada, p. 913–934.

Orkild, P. P., and O'Connor, J. T., 1970, Geologic map of the Topopah Spring quadrangle, Nye County, Nevada: U.S. Geological Survey Geologic Quadrangle Map GQ-849, scale 1:24 000.

Orkild, P. P., Sargent, K. A., and Snyder, R. P., 1969, Geologic map of Pahute Mesa, Nevada Test Site and vicinity, Nye County, Nevada: U.S. Geological Survey Miscellaneous Investigations Series Map I-567, scale 1:48 000.

Parsons, T., and Thompson, G. A., 1991, The role of magma overpressure in supressing earthquakes and topography—Worldwide examples: Science, v. 253, p. 1399–1402.

Pierce, K. L., and Morgan, L. A., 1992, The track of the Yellowstone hot spot—Volcanism, faulting, and uplift, *in* Link, P. K., Kuntz, M. A., and Platt, L. B., eds., Regional geology of eastern Idaho and western Wyoming: Geological Society of America Memoir 179, p. 1–53.

Poole, F. G., Carr, W. J., and Elston, D. P., 1965, Salyer and Wahmonie Formations of southeastern Nye County, Nevada, *in* Contributions to stratigraphy 1965: U.S. Geological Survey Bulletin 1224-A, p. A36–A44.

Rosenbaum, J. G., Hudson, M. R., and Scott, R. B., 1991, Paleomagnetic constraints on the geometry and timing of deformation at Yucca Mountain, Nevada: Journal of Geophysical Research, v. 96, p. 1963–1979.

Sargent, K. A., and Orkild, P. P., 1973, Geologic map of the Wheelbarrow Peak–Rainier Mesa area, Nye County, Nevada: U.S. Geological Survey Miscellaneous Investigations Map I-754, scale 1:48 000.

Sargent, K. A., Noble, D. C., and Ekren, E. B., 1964, Belted Range Tuff of Nye and Lincoln Counties, Nevada: U.S. Geological Survey Bulletin 1224-A, p. 32–36.

Sawyer, D. A., and Sargent, K. A., 1989, Petrologic evolution of divergent peralkaline magmas from the Silent Canyon caldera complex: Journal of Geophysical Research, v. 94, p. 6021–6040.

Scott, R. B., 1990, Tectonic setting of Yucca Mountain, southwest Nevada, *in* Wernicke, B. P., ed., Basin and Range extensional tectonics near the latitude of Las Vegas, Nevada: Geological Society of America Memoir 176, p. 251–282.

Severinghaus, J., and Atwater, T., 1990, Cenozoic geometry and thermal state of subducting slabs beneath western North America, *in* Wernicke, B. P., ed., Basin and Range extensional tectonics near the latitude of Las Vegas, Nevada: Geological Society of America Memoir 176, p. 1–22.

Snyder, D. B., and Carr, W. J., 1984, Interpretation of gravity data in a complex volcano-tectonic setting, southwestern Nevada: Journal of Geophysical Research, v. 89, p. 10 193–10 206.

Stewart, J. H., and Carlson, J. H., 1978, Geologic map of Nevada: U.S. Geological Survey, scale 1:500 000.

Tabor, R. W., Mark, R. K., and Wilson, R. H., 1985, Reproducibility of the K-Ar ages of rocks and minerals—An empirical approach: U.S. Geological Survey Bulletin 1654, 5 p.

Taylor, J. R., 1982, An introduction to error analysis: Mill Valley, California, University Science Books, 269 p.

Taylor, W. J., Bartley, J. M., Lux, D. R., and Axen, G. J., 1989, Timing of Tertiary extension in the Railroad Valley–Pioche transect, Nevada—Constraints from $^{40}Ar/^{39}Ar$ ages of volcanic rocks: Journal of Geophysical Research, v. 94, p. 7757–7774.

Tegtmeyer, K. J., 1990, Regional variation in the Nd and Sr isotopic compositions of Tertiary peralkaline rhyolites from the Great Basin, western U.S. [abs.]: Eos (Transactions, American Geophysical Union), v. 71, p. 1682.

Tegtmeyer, K. J., and Farmer, G. L., 1990, Nd isotopic gradients in upper crustal magma chambers: Evidence for in situ magma–wall-rock interaction: Geology, v. 18, p. 5–9.

U.S. Geological Survey, 1979, Aeromagnetic map of the Timber Mountain area, Nevada: U.S. Geological Survey Open-File Report 79-587, scale 1:62 500.

Vogel, T. A., Noble, D. C., and Younker, L. W., 1983, Chemical evolution of a high-level magma system—The Black Mountain volcanic center: Lawrence Livermore Laboratory Report UCRL-53444, 49 p.

Warren, R. G., 1983, Geochemical similarities between volcanic units at Yucca Mountain and Pahute Mesa—Evidence for a common magmatic origin for volcanic sequences that flank the Timber Mountain caldera, *in* Olsen, C. W., compiler, Proceedings, Second Symposium on the Containment of Underground Nuclear Explosions: Lawrence Livermore Laboratory Report CONF-830882, v. 1, p. 213–244.

Warren, R. G., Byers, F. M., Jr., and Caporuscio, F. A., 1984, Petrography and mineral chemistry of units of the Topopah Spring, Calico Hills, and Crater Flat tuffs, and older volcanic units with an emphasis on samples from USW G-1, Yucca Mountain, Nevada Test Site: Los Alamos National Laboratory Report LA-10003-MS, 78 p.

Warren, R. G., Byers, F. M., Jr., and Orkild, P. P., 1985, Post–Silent Canyon caldera structural setting for Pahute Mesa, *in* Olsen, C. W., and Donohue, M. L., eds., Proceedings, Third Symposium on the Containment of Underground Nuclear Explosions: Lawrence Livermore National Laboratory CONF-850953, v. 2, p. 31–45.

Warren, R. G., McDowell, F. W., Byers, F. M., Jr., Broxton, D. E., Carr, W. J., and Orkild, P. P., 1988, Episodic leaks from Timber Mountain caldera—New evidence from rhyolite lavas of Fortymile Canyon, SW Nevada volcanic field [abs.]: Geological Society of America Abstracts with Programs, v. 20, p. 240.

Warren, R. G., Byers, F. M., Jr., Broxton, D. E., Freeman, S. H., and Hagan, R. C., 1989, Phenocryst abundances and glass and phenocryst compositions as indicators of magmatic environments of large-volume ash flow sheets in southwestern Nevada: Journal of Geophysical Research, v. 94, p. 5987–6020.

Weiss, S. I., Noble, D. C., and McKee, E. H., 1989, Paleomagnetic and cooling constraints on the duration of the Pahute Mesa–Trail Ridge eruptive event and associated magmatic evolution: Journal of Geophysical Research, v. 94, p. 6075–6084.

Wernicke, B. P., 1992, Cenozoic extensional tectonics of the U.S. Cordillera, *in* Burchfiel, B. C., Lipman, P. W., and Zoback, M. L., eds., The Cordilleran orogen: Conterminous U.S.: Boulder, Colorado, Geological Society of America, Geology of North America, v. G-3, p. 553–581.

Wernicke, B. P., Axen, G. J., and Snow, J. K., 1988, Extensional tectonics at the latitude of Las Vegas, Nevada: Geological Society of America Bulletin, v. 100, p. 1738–1757.

MANUSCRIPT RECEIVED BY THE SOCIETY FEBRUARY 17, 1993
REVISED MANUSCRIPT RECEIVED FEBRUARY 15, 1994
MANUSCRIPT ACCEPTED FEBRUARY 24, 1994

Printed in U.S.A.

THIS EXTENDED LAND

Geological Journeys in the Southern Basin and Range

Field Trip Guidebook
Geological Society of America
Cordilleran Section Meeting
Las Vegas, Nevada
1988

Editors

David L. Weide, UNLV
Marianne L. Faber, Lockheed-EMSCO

SPONSORED BY

Department of Geoscience
University of Nevada
Las Vegas, Nevada

A FIELD TRIP GUIDE TO THE GEOLOGY OF BARE MOUNTAIN

Michael D. Carr and Susan A. Monsen
U.S. Geological Survey
345 Middlefield Road
Menlo Park, California 94025

INTRODUCTION

Bare Mountain, southeast of Beatty, Nevada, exposes a faulted and folded, but generally northward-dipping section of upper Proterozoic and Paleozoic miogeoclinal sedimentary rocks (figs. 1 and 2). This isolated mountain edifice, roughly triangular in map view, is bordered on the east by Crater Flat, an asymmetric graben filled by as much as 3.5 km of Cenozoic volcanic and sedimentary rocks (Ackermann and others, in press). Bare Mountain is bordered on the southwest by the northern Amargosa Desert, a broad alluvial valley filled by less than a kilometer of Cenozoic deposits (Healey and Miller, 1972). North of Bare Mountain, a complexly faulted terrane of middle Miocene volcanic and sedimentary rocks rests in low-angle fault contact on the upper Proterozoic and Paleozoic rocks that form Bare Mountain proper. This faulted terrane of Miocene rocks continues westward to form the Bullfrog Hills. Upper Miocene(?) and younger alluvial deposits lap over the faulted middle Miocene rocks farther north. Quaternary alluvial fans lap over bedrock on the west flank of Bare Mountain, but faults disrupt the Quaternary deposits along the eastern range front.

Day 1 of this trip is intended to explore evidence for several hypotheses concerning the geometry and history of a regional, low-angle, extensional (detachment) fault system exposed in Fluorspar Canyon (northern Bare Mountain) and along the south side of the Bullfrog Hills. (The segment of this fault system in Flourspar Canyon is referred to herein as the Fluorspar Canyon fault and, following Ransome and others (1910), the segment along the south side of the Bullfrog Hills is called the Original Bullfrog fault.) This fault system occupies the same structural position as the Boundary Canyon fault in the Funeral and Grapevine Mountains. Our favored hypothesis is that the Grapevine Mountains, Bullfrog Hills, and northernmost Bare Mountain are parts of an extensional allochthon that has moved west-northwest from a breakaway in the vicinity of Bare Mountain, along a system of low-angle normal faults comprising the Boundary Canyon, Original Bullfrog, and Fluorspar Canyon faults. The terrane east of the breakaway consists of less-faulted, nearly flat-lying middle Miocene volcanic and sedimentary rocks forming a dissected plateau northeast of Bare Mountain.

Interpretations of the eastward extent of the Fluorspar Canyon fault and its relationship to faulting at Yucca Mountain, 15 km east of Bare Mountain, are controversial. According to our interpretation, the faults at Yucca Mountain have a different movement history from those in the extensional terrane of northern Bare Mountain and the Bullfrog Hills (see Stop 5). We consider faults at Yucca Mountain to be genetically related to the Crater Flat graben system, a separate structural domain from that in the upper plate of the Fluorspar Canyon fault. No single fault, or group of faults having structural histories in common, has been identified that directly connects the Fluorspar Canyon fault with the eastern range-front fault of Bare Mountain.

The Boundary Canyon-Original Bullfrog-Fluorspar Canyon fault system at the base of the Grapevine-Bullfrog-northern Bare Mountain allochthon cuts successively older stratigraphic units in both the upper and lower plates toward the west. The fault system describes gentle warps along northwest-trending axes forming apparent antiforms in the Funeral Mountains and southern Bullfrog Hills and an intervening apparent synform in the northern Amargosa Desert. It is not known whether the low-angle fault originally was a planar, westward-dipping surface that subsequently was folded, or if it was formed as a corrugated surface having nearly its present geometry.

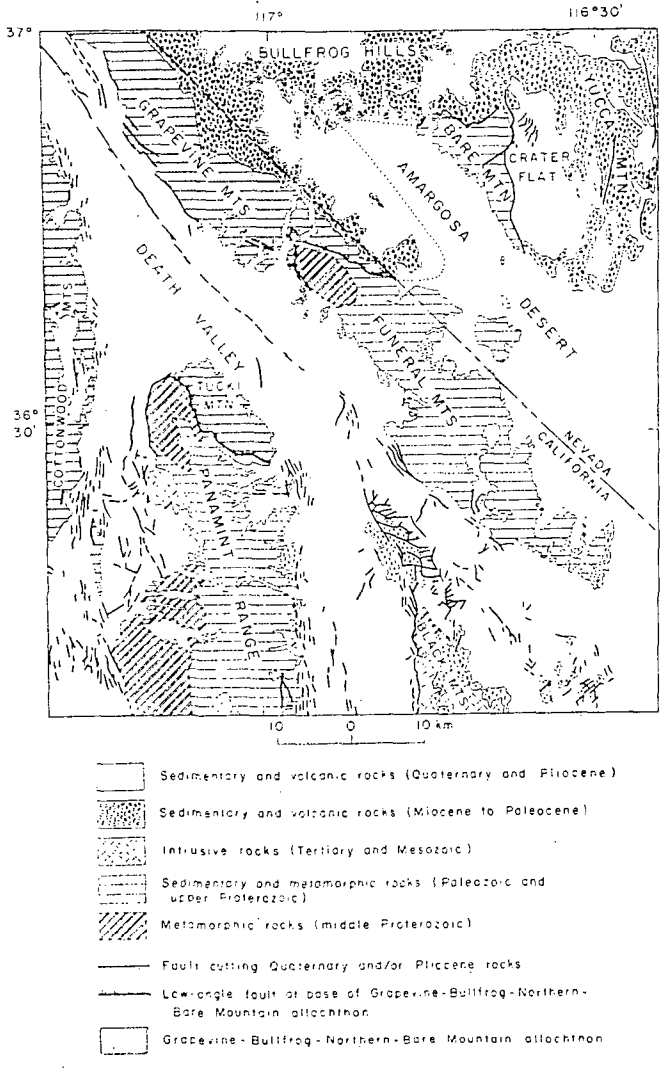

Figure 1. Map of area from Crater Flat to northern Death Valley. Shows one possible correlation of the major low-angle normal fault system between Bare Mountain and the Funeral Mountains, as well as the possible extent of the Grapevine-Bullfrog-Northern Bare Mountain allochthon. For alternative interpretations see Carr (1984) or Hamilton (1987, in press).

The allochthon above the Boundary Canyon fault in the Grapevine Mountains and western Bullfrog Hills consists of faulted blocks of unmetamorphosed upper Proterozoic and Paleozoic sedimentary rocks unconformably overlain by Tertiary volcanic and nonmarine sedimentary rocks (Reynolds, 1969). Farther east in the Bullfrog Hills, where the Original Bullfrog fault has cut higher in the stratigraphic section, the Paleozoic section is cut out and faulted Tertiary rocks form the entire upper plate (Cornwall and Kleinhampl,

1964; Florian Maldonado, written commun., 1986). Listric and high-angle planar faults both are recognized in the upper plate. These faults terminate downward at or merge with the low-angle fault at the base of the extensional allochthon (Ransome and others, 1910; Maldonado, 1985; Florian Maldonado, written commun., 1986; Florian Maldonado and B.P. Hausback, written commun., 1987).

The lower plate, which is exposed in the Funeral Mountains, in two knolls south of the Bullfrog Hills, and at Bare Mountain, contains Proterozoic and Paleozoic rocks that have been ductilely deformed and variably metamorphosed to greenschist and amphibolite facies (Labotka, 1980; Monsen, 1983). Persisting uncertainty surrounds the relationship, if any, between ductile deformation, metamorphism, and Tertiary extension in the region.

Our study of Bare Mountain was done in part as a contribution to geologic framework studies of the proposed U.S. Department of Energy site for disposal of high-level nuclear waste at Yucca Mountain (Interagency Agreement DE-AI08-78ET44802). Hypothetical earthquakes postulated for the eastern range-front fault of Bare Mountain have been used for estimating peak deterministic ground acceleration at the Yucca Mountain site (Rogers and others, 1977; U.S. Dept. of Energy, 1986).

PREVIOUS WORK

Among the earliest geologic studies to include Bare Mountain was the reconnaissance of Ball (1907), who noted the metamorphic rocks at the north end of Bare Mountain and described mesoscopic structures in these rocks. Ransome and others (1910), mapping the Bullfrog mining district, first documented major low-angle normal faulting in the southern Great Basin and described the fault style in the upper plate extensional terrane of the Bullfrog Hills. They correlated the Fluorspar Canyon fault with the Original Bullfrog fault along the south side of the Bullfrog Hills. Cornwall and Kleinhampl (1961, 1964) mapped the Bare Mountain and Bullfrog Hills 15' quadrangles. M.W. Reynolds (1969, unpublished data) mapped the Grapevine Mountains and parts of the Bullfrog Hills.

More recently, Monsen (1983) mapped and discussed the stratigraphy, metamorphism, and structural geology of northwestern Bare Mountain. Swadley and Parrish (in press) mapped surficial deposits in the Bare Mountain 15' quadrangle, and Reheis (1986) studied faulting of surficial deposits along the eastern range front. Other recent studies include those of the northern half of the Bullfrog 15' quadrangle (1:24,000) by Florian Maldonado and B.P. Hausback and of Tertiary rocks in the Bare Mountain 15' quadrangle (1:48,000) by P.P. Orkild. We are grateful to these people for providing preliminary copies of their work, which we have cited to supplement our studies of Bare Mountain (1:24,000).

ROAD LOG

SET ODOMETER TO ZERO

ODOMETER 0.0

Parking lot of the Burro Inn, U.S. Highway 95, Beatty, Nevada. Proceed south from Beatty on Highway 95. The field trip route is covered by the Bare Mountain, Nevada, and Bullfrog, Nevada-California 15' quadrangles.

0.9

Amargosa Narrows. Turn left on Fluorspar Canyon road (graded dirt).

1.7

Turn left on mine road (dirt track). Take left fork at 1.9 mi.

2.1

Stop 1

Beatty Mountain - Hike to the saddle on the south flank of Beatty Mountain, approximately 100 m west of the mine road.

Fluorspar Canyon fault - A gently dipping fault in the saddle on the south flank of Beatty Mountain, the Fluorspar Canyon fault, separates middle Miocene volcanic and sedimentary rocks above from upper Proterozoic and Cambrian metasedimentary rocks below. The exhumed surface (dipping 25° N.) on top of the carbonate rocks south of the saddle reflects the approximate attitude of the fault. In the upper plate of the Fluorspar Canyon fault, Tertiary rocks are tilted moderately eastward in blocks bounded by moderately to steeply northwest-dipping faults. The faults in the upper plate terminate at or merge with the low-angle Fluorspar Canyon fault at depth.

Rocks in the footwall are part of a structurally attenuated section of upper Proterozoic and Cambrian metasedimentary rocks, better exposed in Conejo Canyon (Stop 11). These rocks dip northward in normal stratigraphic order, but large intervals of the stratigraphic section have been cut out along low-angle faults that nearly parallel bedding. The uppermost of these units (Middle Cambrian carbonate rocks) has been intruded by a granitic sill, which is dated as Cretaceous on the basis of U-Th-Pb age data from included zircon (R.E. Zartman, written commun., 1985).

The Fluorspar Canyon fault is interpreted by us as part of a regional, low-angle normal fault system that propagated to the land surface in the Bare Mountain area during the late Miocene. The fault projects westward across the Amargosa Narrows, where it continues as the low-angle Original Bullfrog fault at the base of the extended Tertiary volcanic terrane of the Bullfrog Hills (Ransome and others, 1910). The fault can be traced eastward to the head of Fluorspar Canyon. Where, or whether, the Fluorspar Canyon fault continues farther east is a question to be discussed at the next stop.

Retrace route along the mine road to Fluorspar Canyon road. Turn left on Fluorspar Canyon road.

The style of faulting in the upper plate of the Fluorspar Canyon fault is well displayed on the north side of Fluorspar Canyon.

4.9

Turn left on road to Secret Pass radio facility (graded dirt).

The mine to the south is the Daisy fluorspar mine, which has been mined since 1918 making it one of Nevada's oldest continuously operated mines. The mine explores hydrothermal fluorite deposits that have replaced dolomite and filled cavities along faults in Middle and Upper Cambrian carbonate strata (Cornwall and Kleinhampl, 1964).

7.4

Stop 2

Secret Pass - At this stop, we view the inferred breakaway of the extensional terrane above the Fluorspar Canyon fault to the north, as well as a complex of low-angle faults within the Paleozoic rocks to the south and east. The small ridge of volcanic rocks to the north contains a conformable or paraconformable sequence of middle Miocene tuff and tuffaceous sedimentary units, dipping moderately eastward. To the northeast, this section flattens beneath the volcanic mesas that lead off to the Timber Mountain caldera, the rugged terrain on the northeastern horizon. The middle Miocene geomorphology seems only slightly modified in that area. To the northwest, the same middle Miocene section forms the jumble of fault-bounded blocks that are tilted eastward along northwestward-dipping faults in the upper plate of the

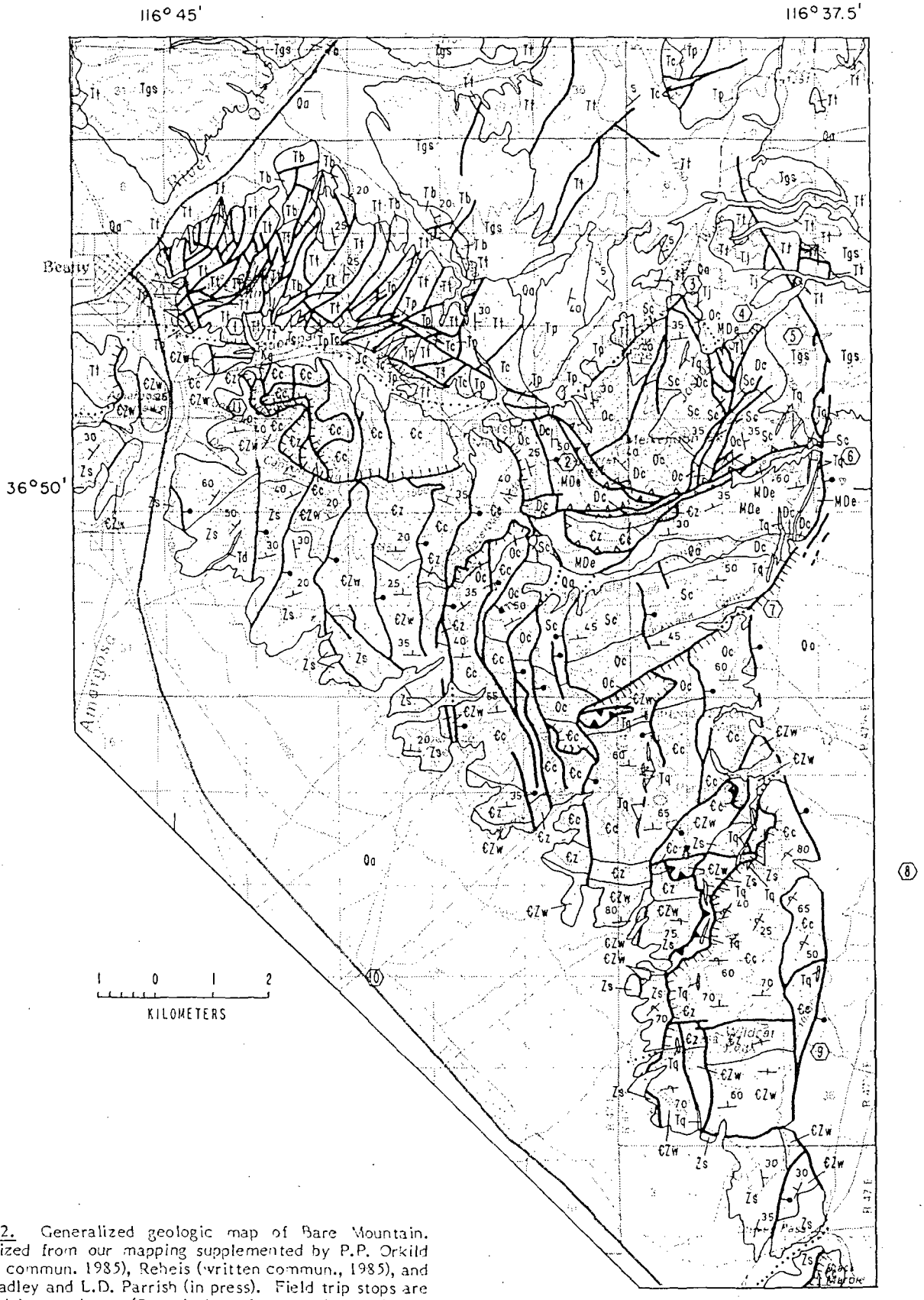

Figure 2. Generalized geologic map of Bare Mountain. Generalized from our mapping supplemented by P.P. Orkild (written commun. 1985), Reheis (written commun., 1985), and W C Swadley and L.D. Parrish (in press). Field trip stops are indicated by number. (Description of map units on facing page.)

DESCRIPTION OF MAP UNITS FOR FIGURE 2

Sedimentary and volcanic rocks

Qa	Alluvial deposits (Quaternary)
Tgs	Gravel of Sober-up Gulch (Miocene)
Tb	Basalt (Miocene)
Tt	Timber Mountain Tuff (Miocene)--includes unnamed bedded tuff unit below the Timber Mountain Tuff
Tp	Paintbrush Tuff (Miocene)
Tc	Crater Flat Tuff (Miocene)
Tj	Joshua Hollow sequence (Miocene)
MDe	Eleana Formation (Mississippian and Devonian?)
Dc	Carbonate rocks (Devonian)
Sc	Carbonate rocks (Silurian)--Lone Mountain Dolomite and Roberts Mountains Formation
Oc	Carbonate and clastic rocks (Ordovician)--Ely Springs Dolomite, Eureka Quartzite, and Pogonip Group
Cc	Carbonate and clastic rocks (Cambrian)--Nopah, Bonanza King, and Carrara Formations
Cz	Zabriskie Quartzite (Cambrian)
CZw	Wood Canyon Formation (Cambrian and upper Proterozoic)
Zs	Stirling Quartzite (upper Proterozoic)

Intrusive rocks

Tq	Quartz latite dikes (Miocene)
Td	Diorite dikes (Oligocene)
Kg	Granitic sill (Cretaceous)

Symbols

45	Strike and dip of layering
——	Fault
——	Oblique slip fault belonging to the set of north-striking faults forming the western wall of the Crater Flat graben (bar and ball on hanging wall)
——	Low-angle fault interpreted as normal fault (hatchures on upper plate)
——	Low-angle fault interpreted as thrust fault (teeth on upper plate)
——	Low-angle fault, sense of movement uncertain (teeth on upper plate)

Fluorspar Canyon fault. The youngest rocks involved in this faulting are basalt inferred to be 10.5 Ma by Carr (1984, p. 58). The basalt is apparently conformable on the sequence of middle Miocene ash-flow tuffs. Nearly flat-lying alluvial fan deposits, which we infer to be upper Miocene on the basis of their similarity to isotopically dated deposits east of Bare Mountain (7.7 to 8.7 Ma, J.K. Nakata, written commun., 1986), lap unconformably over the strongly faulted and tilted middle Miocene rocks north of Bare Mountain. These relationships suggest that much, if not all, of the extension above the Fluorspar Canyon fault occurred between about 10.5 and 7.5 Ma in the Bare Mountain area. The boundary between the strongly deformed extensional terrane to the northwest and the less-deformed plateau to the northeast is the fault on the west side of the small ridge north of this stop. This fault is interpreted as part of the breakaway for the Grapevine-Bullfrog-northern Bare Mountain extensional allochthon.

South and east of Secret Pass, a complex of three low-angle faults repeats (and locally elides) the Paleozoic section. The basal fault places Cambrian strata over Mississippian Antler foreland basin deposits along the south side of the quartzite ridge at Specie Spring. At its west end, this fault along with strata in both its upper and lower plates are folded into an eastward-vergent syncline and apparently is truncated by the middle of the three low-angle faults, which carries Devonian and Mississippian strata in its upper plate. A fault-bounded sliver of Devonian dolomite occurs locally along the middle fault zone. The uppermost of the three low-angle faults places Ordovician carbonate rocks on Mississippian rocks east of Secret Pass. Fault-bounded slivers of Devonian dolomite also occur locally along this fault zone. Southeast of Meikeljohn Peak, all of the low-angle faults merge into a single fault that separates Ordovician through Devonian rocks above from Mississippian rocks below. Near the east edge of the range, this fault is cut by one of a set of quartz latite dikes isotopically dated at about 14 Ma (Carr, 1984; J.K. Nakata, written commun. 1986).

Most of the low-angle faults in the vicinity of Secret Pass repeat stratigraphic section, but it is difficult to establish whether they formed as thrust faults or as low-angle normal faults cutting a previously deformed terrane. The basal low-angle fault occupies the same structural position as a thrust fault at the south end of Bare Mountain (Stop 8), but modifications of the low-angle fault surface by normal faults have obscured the initial fault geometry in the Specie Spring area. The middle low-angle fault, south of Secret Pass, apparently cuts the folded basal fault and, therefore, appears to be younger than the basal fault. The uppermost of the three low-angle faults cuts upward through the stratigraphic section in its upper plate toward the east. East of the point where the three faults merge, the fault cuts at approximately a constant stratigraphic level in the lower plate. These relationships are suggestive of a thrust fault geometry wherein the upper plate of the uppermost low-angle fault was cut from the ramp area of an imbricate thrust system and moved generally eastward, up and over a flatter part of the thrust system that roughly paralleled layering in the lower plate. The low-angle fault complex formed, and all of the movement at its east end occurred, before the intrusion of the 14-Ma quartz latite dikes. Movement on northwest-dipping, high-angle normal faults in the vicinity of Meikeljohn Peak, which are truncated down dip at the uppermost of the low-angle faults, apparently occurred after intrusion of the quartz latite dikes (see Stop 4). We currently favor an interpretation in which the complex of low-angle faults in the vicinity of Secret Pass formed as thrust faults, probably during the Mesozoic, but parts of each of these faults have been reactivated during the Tertiary as extensional faults.

Retrace route down road from Secret Pass radio facility.

8.6

Turn right on road to Tates Wash (graded dirt). Follow left branch of road at 10.3 mi. Follow right branch of road at 10.4 mi.

South of Tates Wash, Tertiary tuffaceous sedimentary rocks and tuff are faulted against Paleozoic rocks along a fault that dips 40° to 45° N. (Cornwall and Kleinhampl, 1961).

10.8

Stop 3.

Tates Wash - Here we will discuss the relationship between the Fluorspar Canyon fault and the eastern range-front fault. The fault between Paleozoic and middle Miocene rocks along the south side of Tates Wash generally is mapped as the eastern continuation of the Fluorspar Canyon fault. Cornwall and Kleinhampl (1961) connected this fault around the northeast corner of Bare Mountain with a north-striking fault separating lower Miocene deposits from the Paleozoic rocks in Joshua Hollow. Other workers (e.g., Hamilton, 1987) recently have inferred that the Flourspar Canyon fault

continues around the northeastern part of Bare Mountain to join the eastern range-front fault, and that together these faults form a system of detachment faults on top of a lens of mid-crustal rocks forming the Bare Mountain massif.

On the basis of our mapping, we conclude that displacement on the Fluorspar Canyon fault dies out to the east and that movement on faults in Fluorspar Canyon, Tates Wash, and Joshua Hollow ceased in the late Miocene, while the range-front fault is currently active. Because of their contrasting histories and geometries, we conclude that the Fluorspar Canyon and eastern range-front faults belong to separate fault systems.

Continue straight ahead.

11.4
Turn left on dirt track heading east down the alluvial fan terrace.

Stop 4.

Joshua Hollow - Walk to the outcrop of Tertiary gravels faulted against Mississippian rocks on the south side of wash. These gravels are part of a sequence of sedimentary and volcanic deposits inferred to be of lower Miocene age. The gravels rest stratigraphically on crystal tuff to the west, which, in turn, rests on lacustrine mudstone. The lacustrine unit is cut by a quartz latite dike dated at about 13.9 Ma (J.K. Nakata, written commun., 1986). The Tertiary sequence in Joshua Hollow is lithologically similar to deposits that rest disconformably on the Oligocene Titus Canyon Formation and are below the middle Miocene Crater Flat Tuff in the eastern Grapevine Mountains (Reynolds, 1969), within the extensional allochthon.

The Tertiary gravels dip eastward about 30°, abutting Paleozoic rocks along a moderately steep, westward-dipping fault. The quartz latite dike in the lacustrine unit down section has been rotated eastward from vertical about the same number of degrees that the gravel beds have been rotated eastward from horizontal, suggesting that faulting and tilting of the lower Miocene rocks occurred after 14 Ma. The west-dipping fault can be traced southward along strike until it is cut by a steeply northwestward-dipping normal fault. That fault, in turn, is lapped over by and does not offset upper Miocene alluvial fan deposits that contain an ash-fall tuff isotopically dated as 7.7 to 8.7 Ma (J.K. Nakata, written commun., 1986). In contrast, the range-front fault cuts the upper Miocene deposits, as well as Pliocene and Quaternary deposits along the east side of Bare Mountain (Reheis, 1986).

Return to vehicles, and continue on track down wash and around to the east side of Bare Mountain (rough dirt track--drive carefully).

13.0

Stop 5

Northern Crater Flat - View stop for Crater Flat and Yucca Mountain.

Crater Flat is an asymmetric graben. Gravity and seismic-refraction data (Healey and Miller, 1972; U.S. Geological Survey, 1984, fig. 2; Sutton, 1985) have been interpreted as indicating that the graben continues southward into the Amargosa Desert (e.g. Snyder and Carr, 1984), but surface expression of the structure and obvious Quaternary activity seems to be confined to Crater Flat. Active faults are recognized at Bare Mountain on the west side of the graben (Reheis, 1986) and at Yucca Mountain on the east (Swadley and others, 1984); a Quaternary basalt field has erupted within the graben structure.

Yucca Mountain, on the east side of Crater Flat, is a volcanic plateau that is cut by numerous, steeply westward-dipping faults. A persisting question concerns the geometry of these faults at depth. Scott and others (1984) interpreted the principal faults at Yucca Mountain as listric, and it has become popular to speculate that these faults flatten into a "detachment" fault at the base of the Tertiary section, above the underlying Paleozoic rocks, a few kilometers beneath Yucca Mountain.

However, the layering within the major fault-bounded blocks forming Yucca Mountain dips uniformly to the east at about 10° to 15° (Scott and Bonk, 1984). Such uniform tilting of imbricate fault blocks is more likely to indicate planar faulting rather than listric faulting according to Wernicke and Burchfiel (1982). The spatial coincidence of Quaternary volcanism with the active graben system is suggestive of a deep-seated structural system. We certainly should consider the possibility that the principal faults at Yucca Mountain are planar-rotational faults, penetrating deep into the Paleozoic rocks before they are accommodated at depth by some sort of detachment zone (whether that be the base of the crust, the ductile-brittle transition zone, or some low-angle fault in the upper crust analogous to that north of Bare Mountain or those in the Death Valley area). The depth at which the steeply-dipping faults at Yucca Mountain are geometrically and kinematically accommodated and the nature of such accommodation remain unknown.

Carr (1984) concluded that a major pulse of extensional faulting occurred in the Yucca Mountain and Crater Flat areas between about 11.5 and 12.9 Ma, based on the presence of an angular unconformity in the Tertiary sections of about that age. Furthermore, monolithologic breccia deposits of Paleozoic rocks occur between 11.5- and 12.9-Ma tuff units in a drill hole in Crater Flat (Carr and Parrish, 1985). An unconformity also occurs at the base of an 11.5-Ma tuff northeast of Bare Mountain on the west side of the Crater Flat graben, but the 11.5-Ma tuff is concordant on older units farther to the west. Apparently, the 11.5-to-12.9-Ma event is characteristic of the Crater Flat graben, and deformation north and west of Bare Mountain occurred at different times and in a different structural domain. Tectonic activity in the Crater Flat graben continues, whereas faults in the extensional terrane north and west of Bare Mountain appear to be mostly inactive.

Continue along dirt track toward the south.

14.8

Stop 6 (optional)

Northern Bare Mountain low-angle fault complex - The quartz latite dike near the mouth of the canyon to the west is one of a set of dikes dated at about 14 Ma (Carr, 1984; J.K. Nakata, written commun., 1986). On the north slope of the canyon, the dike cuts a low-angle fault along which Silurian carbonate rocks rest on Mississippian shale. It is this fault that bifurcates westward to form the low-angle fault complex described at Stop 2. Because movement along this segment of the fault ceased long before movement on the Fluorspar Canyon fault began, the Fluorspar Canyon fault cannot connect with the range-front fault along this fault.

16.1
Mouth of Tarantula Canyon. Continue south along range front (poorly graded dirt road).

17.4
Turn right on road to Chuckwalla Canyon (poorly graded dirt).

18.1

Stop 7

Chuckwalla Canyon - Walk northeast (about 100 m) to the prospect pit inclined along the contact between alluvium and bedrock.

The range-front fault is exposed in this pit, where it dips about 35° southeast and separates older Pleistocene

alluvial fan deposits from bedrock (Reheis, 1986). A vein of amorphous silica deposited in the fault zone is exposed in the pit several centimeters above the principal fault surface. Slickensides on the vein attest to at least two episodes of faulting--one which formed the fracture along which the vein was deposited and another which scribed the surface of the vein. The vein was isotopically dated as a minimum of 350 ka (Reheis, 1986). The attitude of the slickensides suggests that the last movement along this part of the range-front fault was dip slip.

To the southwest, this gently southeastward-dipping segment of the range-front fault leaves the range front and cuts into bedrock. The fault continues along the south wall of Chuckwalla Canyon to the head of the canyon, where it bends abruptly into a north-striking fault segment that dips about 65° east. Bedrock units in the hanging wall are displaced about 1 km toward the south along the fault in Chuckwalla Canyon. To the northeast, the gently southeast-dipping segment of the range-front fault also bends into a more northerly striking segment, and it apparently steepens as it cuts away from the bedrock contact and into alluvial materials. The geometric constraints imposed by the bends in the range-front fault surface require a strong component of right-lateral strike-slip displacement on the steeply eastward-dipping fault segments, whereas the gently southeastward-dipping fault segment should have nearly pure dip-slip displacement.

Retrace route southward along Chuckwalla Canyon road and continue south along range-front road.

19.5
Intersection with Sterling mine road (graded dirt). Turn left.

20.1

Stop 8

Panama thrust fault - View stop.

The open pit mine along the range front to the west is in a disseminated gold deposit, apparently associated with a thrust fault placing upper Proterozoic clastic rocks over Middle Cambrian carbonate rocks. The thrust fault is exposed at the mine, on the range crest above the mine, and on the west side of the range, but has been dropped below the surface along a normal fault in the canyon west of the mine. This thrust fault occupies the same structural position as the basal fault in the low-angle fault complex at the north end of the range, but we do not know whether the two fault segments are parts of a single thrust fault. A klippe of Lower Cambrian clastic rocks, which also occupies the same structural position, rests in low-angle fault contact on Ordovician carbonate rocks at the range crest in central Bare Mountain. If all of these thrust segments are correlative, then toward the north, the thrust cuts upward through the stratigraphic section in both its upper and lower plates. The thrust fault segment in the southern part of the range decreases in displacement as it is traced to the south.

The sense of overturning of the stratigraphic sequence above and below the thrust fault in the southern part of the range is consistent with a ramp or fold-fault geometry in which the fault surface cuts upward toward the north through a north-facing fold. Thrust faults or fold faults that face toward the hinterland are unusual in the Cordilleran thrust belt. However, a map-scale fold couple, overturned to the west, does occur in the Grapevine Mountains in the upper plate of the Boundary Canyon fault (Reynolds, 1969). Numerous segments of thrust faults having stratigraphic throws similar to those at Bare Mountain are recognized in the surrounding region (Stewart and others, 1966). Many of these cut upward toward the foreland, but others, such as the thrust fault at the south end of Bare Mountain, are more probably backthrusts. One should be cautious in correlating thrust faults throughout this region and in using correlations of thrust faults as a principal basis for palinspastic reconstructions.

Continue south along Sterling mine road.

24.2
Turn right on dirt track toward Wildcat Peak. Follow detour northward around wash out. Follow left branch of track at 24.7 mi. Follow right branch of track at 25.0 mi.

25.2

Stop 9

Range-front fault - Walk to prospect pit at foot of range (about 100 m).

The range-front fault exposed in this prospect pit dips about 60° east. Reheis (1986) advanced a series of arguments based on this exposure that require at least two episodes of Quaternary offset; the latest of these may have been during the Holocene.

The Cambrian carbonate rocks in the footwall of the range-front fault are themselves faulted against Lower Cambrian quartzite farther west along a splay of the range-front fault system, which parallels the fault exposed in the exploration pit. The fault separating the carbonate rocks from the quartzite cannot have pure dip-slip displacement, because there are no equivalent Cambrian carbonate rocks in the footwall up dip along this fault from those carbonate rocks exposed in the hanging wall at the range front. Furthermore, it is unlikely that such carbonate rocks ever occurred in the footwall in a position that would reasonably permit pure dip-slip displacement on the fault, because the strata in the footwall are vertical to overturned northward. The nearest Cambrian carbonate units in the footwall are a kilometer or more to the north. These relationships suggest a strong component of right-lateral strike slip along the splay of the range-front fault system separating the carbonate rocks from the quartzite.

The eastward-dipping segment of the range-front fault exposed at this stop terminates northward against the southeastward-dipping segment of the range-front fault exposed at the mouth of Chuckwalla Canyon. The eastern range front of Bare Mountain is not controlled by a single, throughgoing fault surface, but rather is a composite fault system made up of steeply eastward-dipping and gently southeastward-dipping segments. There apparently is a strong component of right-lateral, strike-slip along the steeply eastward-dipping fault segments, while the gently southeastward-dipping segments have nearly pure dip-slip displacement.

26.2
Retrace route to Sterling mine road. Turn south on mine road.

29.7
Intersection with U.S. Highway 95. Turn right.

35.1

Stop 10.

Carrara townsite - View stop.

The Carrara townsite resulted from an abortive attempt to quarry marble from Lower and Middle Cambrian units at Bare Mountain during the early 1900s. The marble was too strongly fractured and weathered to be marketable.

A remarkably complete upper Proterozoic and Paleozoic miogeoclinal section, dipping to the north, is exposed along the range. A set of north-striking, steeply eastward-dipping faults apparently offsets younger parts of the stratigraphic section southward against older parts as successive faults are crossed in the direction of dip

(eastward). These faults form the western wall of the Crater Flat graben. Several such faults cut a diorite dike isotopically dated as about 26 Ma (R.J. Fleck, written commun., 1985) in the northwest part of Bare Mountain. In the southeast part of the range, a fault of this set is cut by one of the 14-Ma quartz latite dikes. At a second locality, another of the quartz latite dikes is cut by this same fault, but the dike is not offset as much as the country rock. The steeply east-dipping segments of the active range-front fault system are part of this fault set, and other faults in the set are truncated by the system of low-angle normal faults at the north end of the range. This steeply east dipping fault set, which apparently is the oldest set of extensional faults at Bare Mountain, has had a complex history of reactivation since it was formed sometime before 14 Ma.

The Bullfrog Hills can be seen to the northwest. (The view is better several miles father north along highway 95.) The Original Bullfrog fault (Ransome and others, 1910), westward extension of the Fluorspar Canyon fault, occurs along the south edge of these hills, forming the base of the Grapevine-Bullfrog-northern Bare Mountain extensional allochthon in the Bullfrog Hills. Two light-colored knolls are visible in the valley southwest of Bullfrog Mountain. These hills expose amphibolite-facies upper Proterozoic metasedimentary rocks, which are part of the lower plate of the low-angle fault system, as are the metamorphosed Upper Proterozoic and Paleozoic rocks at Bare Mountain. Slivers of unmetamorphosed Paleozoic rocks, as much as several kilometers long, occur locally in the low-angle fault zone between the faulted blocks of Tertiary volcanic and sedimentary rocks in the upper plate extensional terrane and the high-grade metamorphic rocks in the lower plate (Ransome and others, 1910; Cornwall and Kleinhampl, 1964; Florian Maldonado, written commun., 1986). We interpret these slivers as pieces of the unmetamorphosed Paleozoic section from the base of the Grapevine Mountain block that were spalled off along the low-angle fault zone as the Grapevine Mountain block moved west-northwestward away from Bare Mountain. The low-angle fault surface forms an apparent antiform trending northwest from Bare Mountain through the exposures of metamorphic rocks south of Bullfrog Mountain.

Continue northwest along U.S. 95.

42.3
Mouth of Fluorspar Canyon. Turn right on Fluorspar Canyon road.

42.4
Turn right on dirt track heading southward across the alluvial fans east of the Amargosa River.

42.7
Turn left on track to Conejo Canyon. Follow right branch of track at 43.3 mi.

43.4

Stop 11

Conejo Canyon - The north wall of Conejo Canyon exposes a system of anastamosing low-angle normal faults that severely attenuate an upper Proterozoic and Cambrian section in the lower plate of the Fluorspar Canyon fault (Monsen, 1983). The structurally lowest fault in this system, the Conejo Canyon fault, is located at the top of the continuous orange-brown weathering dolomite unit exposed on the north wall and at the head of Conejo Canyon. The Conejo Canyon fault continues eastward to the vicinity of the Daisy mine in Fluorspar Canyon. The low-angle fault system in Conejo Canyon elides some 1400 m of stratigraphic section within the block of upper Proterozoic and Cambrian rocks between the Conejo Canyon and Fluorspar Canyon faults. The Conejo Canyon fault clearly truncates some of the faults belonging to the set of steeply eastward-dipping faults described at Stop 10, both in its upper and lower plates. Other faults belonging to the steeply eastward-dipping set flatten either upward or downward to merge with the low-angle faults in Conejo Canyon, suggesting continued activity on part of the steeply eastward-dipping fault system synchronous with movement on the low-angle faults. Both the system of low-angle faults and the steeply eastward-dipping faults cut ductile fabrics and mesoscopic structures in the metamorphic rocks.

The rocks in the Conejo Canyon area are the highest grade metamorphic rocks exposed at Bare Mountain. Lower or Middle Cambrian pelitic rocks in the upper plate of the Conejo Canyon fault near the ridge crest at the head of Conejo Canyon have staurolite-bearing mineral assemblages, which indicate amphibolite-facies metamorphism (Monsen, 1983). The upper Proterozoic and Lower Cambrian quartzofelspathic rocks structurally below the Conejo Canyon fault lower in the canyon contain biotite ± garnet assemblages, indicating at least garnet-grade greenschist facies metamorphism. Monsen (1983) concluded that the metamorphism and ductile deformation predated extensional faulting in the Bare Mountain area. In Dry Canyon, immediately south of Conejo Canyon, ductile fabrics and mesoscopic structures are cut by an unmetamorphosed diorite dike (Monsen, 1983), which has yielded a conventional K-Ar ages for hornblende of about 26 Ma and for biotite of about 17 Ma (J.C. VonEssen, written commun., 1985). Muscovite and biotite from the Wood Canyon Formation at the mouth of Dry Canyon yielded conventional K-Ar ages of about 52 Ma and 46 Ma, respectively (J.C. VonEssen, written commun., 1985).

We contend that extensional faults in the Bare Mountain area formed under brittle upper crustal conditions. The metamorphic rocks at Bare Mountain were deformed under ductile conditions deeper in the crust, probably during the Mesozoic. These rocks already had been uplifted to upper crustal levels before they finally were exposed by brittle extensional faulting during the Miocene. The low-angle fault system at the base of the Grapevine-Bullfrog-northern Bare Mountain extensional allochthon broke to the surface in the vicinity of Bare Mountain. This fault system apparently cut to deeper structural levels toward the west, and it may have involved rocks that still remained deep enough during the Tertiary to have undergone some metamorphism and ductile deformation during extension. The importance of Mesozoic dynamothermal events in this region, however, should not be overlooked in the flood of popular models explaining Tertiary tectonism.

Retrace route back to U.S. 95. Turn right and return to Beatty.

REFERENCES CITED

Ackermann, H.D., Mooney, W.D., Snyder, D.B., and Sutton, V.D., in press, Preliminary interpretation of seismic-refraction and gravity studies west of Yucca Mountain, Nevada and California, in Carr, M.D., and Yount, J.C., eds., Short contributions to the geology and hydrology of a potential nuclear waste disposal site at Yucca Mountain, southern Nevada: U.S. Geological Survey Bulletin 1790.

Ball, S.H., 1907, A geologic reconnaissance in southwestern Nevada and eastern California: U.S. Geological Survey Bulletin 308, 218 p.

Carr, W.J., 1984, Regional structural setting of Yucca Mountain, southwestern Nevada, and late Cenozoic rates of tectonic activity in part of the southwestern Great Basin, Nevada and California: U.S. Geological Survey Open-file Report 84-854, 109 p.

Carr, W.J., and Parrish, L.D., 1985, Geology of drill hole VH-2, and structure of Crater Flat, southwestern Nevada: U.S. Geological Survey Open-file Report 85-475, 41 p.